Targeting monoamine oxidase A-regulated TAM polarization for cancer immunotherapy

Yu-Chen Wang
University of California, Los Angeles
Xi Wang
University of California, Los Angeles
Jiaji Yu
University of California, Los Angeles
Feiyang Ma
University of California, Los Angeles
Zhe Li
University of California, Los Angeles
Yang Zhou
Department of Microbiology, Immunology and Molecular Genetics. University of California, Los Angeles, CA 90095, United States.
Samuel Zeng
University of California, Los Angeles
Xiaoya Ma
University of California, Los Angeles
Yanruide Li
University of California, Los Angeles
Adam Neal
University of California, Los Angeles
Jie Huang
University of California, Los Angeles
Angela To
University of California, Los Angeles
Nicole Clarke
University of California, Los Angeles
Sanaz Memarzadeh
University of California, Los Angeles
Matteo Pellegrini
Molecular Cell and Developmental Biology, College of Life Sciences, University of California Los Angeles, Los Angeles, CA
Lili Yang (liliyang@ucla.edu)

University of California, Los Angeles

Article

Keywords: TAMs, MAO-A, MAOIs, cancer immunotherapy

Posted Date: July 9th, 2020

DOI: https://doi.org/10.21203/rs.3.rs-38471/v1

Version of Record: A version of this preprint was published at Nature Communications on June 10th, 2021. See the published version at https://doi.org/10.1038/s41467-021-23164-2.

Abstract

Targeting tumour-associated macrophages (TAMs) is a promising strategy to modify the immunosuppressive tumour microenvironment and improve cancer immunotherapy. Monoamine oxidase A (MAO-A) is an enzyme best known for its function in the brain; small molecule MAO inhibitors (MAOIs) are clinically used for treating neurological disorders. Here we observed MAO-A induction in mouse and human TAMs. MAO-A-deficient mice exhibited decreased TAM immunosuppressive functions corresponding with enhanced antitumour immunity. MAOI treatment induced TAM reprogramming and suppressed tumour growth in preclinical mouse syngeneic and human xenograft tumour models. Combining MAOI and anti-PD-1 treatments resulted in synergistic tumour suppression. Clinical data correlation studies associated high intratumoural MAOA expression with poor patient survival in a broad range of cancers. We further demonstrated that MAO-A promotes TAM immunosuppressive polarization via upregulating oxidative stress. Together, these data identify MAO-A as a critical regulator of TAMs and support repurposing MAOIs for TAM reprogramming to improve cancer immunotherapy.

Introduction

Over the past decade, cancer immunotherapy has achieved significant breakthroughs. In particular, immune checkpoint blockade (ICB) therapy has yielded remarkable clinical responses and revolutionized the treatment of many cancers [1]. So far, the FDA has approved cytotoxic T- lymphocyte antigen 4 (CTLA–4) and programmed cell death protein 1/ligand 1 (PD–1/PD-L1) blockade therapies for treating more than 10 different malignancies [2, 3]; however, only a small fraction of cancer patients respond to these therapies [4, 5, 6]. Most ICB therapies work through enhancing antitumour $CD8^+$ T cell responses, which can be greatly limited by the immunosuppressive tumour microenvironment (TME) [7]. Tumour-associated macrophages (TAMs), a key component of the immunosuppressive TME, dampen T cell antitumour reactivity in the majority of solid tumours [8, 9, 10, 11, 12, 13, 14, 15]. Growing evidence suggests that TAMs are responsible for inhibiting antitumour T cell reactivity and limiting the ICB therapy efficacy, making TAMs potential targets for reversing the immunosuppressive TME and improving cancer immunotherapy [16, 17, 18].

TAMs mature from bone marrow-derived circulating monocytes. These monocytes are recruited to the tumour sites, exposed to chemokines and growth factors in the TME, and subsequently differentiate into TAMs [19, 20, 21, 22]. Depending on the surrounding immune environment, macrophages can be polarized toward an immunostimulatory phenotype by pro- inflammatory stimuli (e.g., IFN-γ) or toward an immunosuppressive phenotype by anti- inflammatory stimuli (e.g., IL–4 and IL–13) [23]. Although a binary polarization system is commonly used in macrophage studies, in most large-scale transcriptome analyses, TAMs showed a continuum of phenotypes expressing both immunostimulatory and immunosuppressive markers in addition to the extreme ends of polarization [23, 24, 25]. These mixed phenotypes and polarization states suggest the complexity of the TME and the residential TAM functionality. As a tumour develops, the enrichment of IL–4 and IL–13 produced by tumour cells and

$CD4^+$ T cells in the TME results in the polarization of TAMs towards an immunosuppressive phenotype, that promotes tumour growth, malignancy, and metastasis [23, 26, 27, 28, 29, 30]. In established solid tumours, TAMs predominately exhibit an immunosuppressive phenotype, evidenced by their production of anti-inflammatory cytokines and arginase–1 (Arg1), as well as their expression of mannose receptor (CD206) and scavenger receptors [31, 32, 33]. Through metabolizing L-arginine via Arg1, TAMs can directly suppress cytotoxic $CD8^+$ T cell responses [34, 35]. Mannose receptor (CD206) expressed by TAMs can impair cytotoxicity of $CD8^+$ T cells by suppressing CD45 phosphatase activity [36]. In addition, TAMs can inhibit T cell activities through immune checkpoint engagement by expressing the ligands of the inhibitory receptors PD–1 and CTLA–4. For example, PD-L1 and PD-L2 expressed on TAMs interact with PD–1 of T cells to directly inhibit TCR signaling, cytotoxic function, and proliferation of $CD8^+$ T cells [31]. These characteristics of TAMs make them potential targets for reversing the immunosuppressive TME to augment antitumour immunity.

Although the predominant phenotype of TAMs in established solid tumours is immunosuppressive, polarization is not fixed. Plasticity, one of the key features of TAMs, enables TAMs to change their phenotype in solid tumours and thereby providing a therapeutic window [37,

38. Repolarizing/reprogramming TAMs from an immunosuppressive and tumour-promoting phenotype toward an immunostimulatory and tumouricidal phenotype has thus become an attractive strategy in immunotherapy [27]. Preclinical and clinical studies are ongoing, evaluating TAM-repolarizing reagents (e.g., CD40 agonists, HDAC inhibitors, PI3Kγ inhibitors, creatine, etc.) for improving ICB therapy; certain efficacies have been reported [17, 29, 31, 39, 40, 41, 42]. Therefore, the search for new molecules regulating TAM polarization and the development of new combination treatments targeting TAM reprogramming are an active direction of current cancer immunotherapy studies.

Monoamine oxidase A (MAO-A) is an outer mitochondrial membrane-bound enzyme encoded by the X-linked *MAOA* gene. MAO-A is best known for its function in the brain, where it is involved in the degradation of a variety of monoamine neurotransmitters, including serotonin, dopamine, epinephrine, and norepinephrine. Through regulating the availability of serotonin, MAOA modulate neuronal activities thereby influencing mood and behavior in humans [43, 44, 45, 46, 47]. Through regulating the availability of dopamine and the abundance of dopamine breakdown byproduct hydrogen peroxide (H_2O_2; hence oxidative stress), MAO-A is involved in multiple neurodegenerative diseases, including Parkinson's disease (PD) [48, 49]. FDA-approved small- molecule MAO inhibitors (MAOIs) are currently available for the treatment of neurological disorders, including depression and PD [47, 49, 50, 51, 52, 53, 54, 55]. However, the functions of MAO-A outside of the brain are largely unknown. In this study, we investigated the role of MAO-A in regulating TAM polarization and evaluated the possibility of repurposing MAOIs for reprogramming TAMs and improving cancer immunotherapy, using knockout and transgenic mice, preclinical mouse syngeneic and human xenograft tumour models, as well as human TAM and clinical data correlation studies.

Results

MAO-A-deficient mice show reduced tumour growth associated with altered TAM polarization

In a search for new molecules regulating TAM reprogramming, we inoculated C57BL/6J mice with syngeneic B16-OVA melanoma tumours, isolated TAMs, and assessed TAM gene expression profiles. Monocytes isolated from tumour-free and tumour-bearing mice were included as controls. In addition to changes in classical genes involved in regulating macrophage immune responses, we observed the induction of a *Maoa* gene in TAMs (Fig. 1a), suggesting that MAO-A may be involved in modulating TAM activities.

To study the role of MAO-A in antitumour immunity *in vivo*, we used MAO-A-deficient mice that carry a hypomorphic MAO-A mutant [56]. Although a degree of *Maoa* expression leakage in the brain had been previously reported in these mice [56], analysis of their immune system showed a nearly complete ablation of MAO-A expression in major lymphoid organs including spleen and bone marrow (BM) (Supplementary Fig. 1a). Since we focused on immune cells in this study, we denote these mice as *Maoa* knockout (KO) mice. When challenged with B16-OVA melanoma cells (Fig. 1b), tumour growth in *Maoa* KO mice was significantly suppressed compared to that in *Maoa* wildtype (WT) mice (Fig. 1c,d). Although similar levels of TAMs (gated as $CD45.2^+CD11b^+Ly6G^-Ly6C^{-/low}F4/80^+$ cells) were detected in *Maoa* WT and *Maoa* KO mice (Supplementary Fig. 1b,c), compared to their WT counterparts, TAMs isolated from *Maoa* KO mice exhibited a less immunosuppressive phenotype, indicated by their decreased expression of immunosuppressive markers (i.e., CD206; Fig. 1e), and their increased expression of immunostimulatory molecules (i.e., CD69, CD86, and MHC class II I-Ab; Fig. 1f-h). Further analysis showed that TAMs from *Maoa* KO mice expressed reduced levels of immunosuppression- associated genes (i.e., *Mrc1*, *Chi3l3*, and *Arg1*; Fig. 1i) and increased levels of pro-inflammatory cytokine genes (i.e., *Il6*, *Tnfa*, and *Ccl2*; Fig. 1j). Corresponding to the altered TAM polarization in *Maoa* KO mice, tumour-infiltrating $CD8^+$ T cells in these mice showed enhanced activation (i.e., increased production of Granzyme B; Supplementary Fig. 1d). Single-cell RNA sequencing (scRNAseq) analysis was performed on tumour infiltrating immune cells isolated from *Maoa* WT and *Maoa* KO mice (Fig. 1k and Supplementary Fig. 1e,f). UMAP analysis of extracted TAMs showed a reduced immunosuppressive phenotype in *Maoa* KO mice, with an increased ratio of $Mrc1^{low}Cd86^{high}$ cells to $Mrc1^{high}Cd86^{low}$ cells (Fig. 1l and Supplementary Fig. 1g). Gene expression profile analysis confirmed a reduction of TAMs expressing immunosuppressive genes (i.e., *Mrc1* and *Chi3l3*; Fig. 1m) and an enrichment of TAMs expressing immunostimulatory genes (i.e., *Ccl2*, *Ccl7*, *Cd86*, *H2-Aa*, and *H2-Ab1*; Fig. 1n) in *Maoa* KO mice. These data strongly indicate that MAO-A is involved in regulating TAM polarization thereby modulating antitumour immunity.

MAO-A directly regulates TAM polarization and influences TAM-associated T cell antitumour reactivity

In our *Maoa* KO mice tumour challenge study, MAO-A deficiency impacted both immune and non-immune cells (Fig. 1b). To determine whether MAO-A directly regulates immune cells, we conducted a BM transfer experiment wherein BM cells harvested from *Maoa* WT or KO mice were adoptively transferred into BoyJ

(CD45.1) WT recipient mice followed by B16-OVA tumour challenge (Fig. 2a). In this experiment, MAO-A deficiency comparison was confined to immune cells. MAO-A deficiency in immune cells resulted in suppressed tumour growth (Fig. 2b,c), altered TAM polarization (i.e., downregulation of immunosuppressive markers such as CD206, Fig. 2d; and upregulation of immunostimulatory markers such as CD69, CD86, and MHC class II I-Ab; Fig. 2e,f and Supplementary Fig. 2a), and enhanced tumour-infiltrating $CD8^+$ T cell activation (i.e., increased production of cytotoxic molecules such as Granzyme B; Supplementary Fig. 2b), indicating that MAO-A directly regulates immune cell antitumour activity, in particular TAM polarization and T cell antitumour reactivity.

To further study whether MAO-A acts as a macrophage autonomous factor directly regulating TAM polarization and thereby influencing antitumour immunity, we performed a macrophage adoptive transfer tumour experiment. BM cells were harvested from *Maoa* WT and KO mice then cultured into bone marrow-derived macrophages (BMDMs). These *Maoa* WT or KO BMDMs were then mixed with B16-OVA melanoma cells and subcutaneously (s.c.) injected into BoyJ WT recipient mice to establish solid tumours (Fig. 2g). In this study, MAO-A deficiency comparison was confined to TAMs. Suppressed tumour growth (Fig. 2h,i), downregulated expression of TAM immunosuppressive markers (i.e., CD206; Fig. 2j), upregulated expression of TAM immunostimulatory markers (i.e., CD69 and CD86; Fig. 2k,l), and enhanced tumour- infiltrating $CD8^+$ T cell reactivity (i.e., increased production of Granzyme B; Fig. 2m) were observed in mice receiving *Maoa* KO BMDMs. Collectively, these *in vivo* studies demonstrate that MAO-A acts as an autonomous factor directly regulating TAM polarization, and thereby influencing T cell antitumour reactivity and impacting tumour growth.

MAO-A promotes macrophage immunosuppressive polarization

To study MAO-A regulation of macrophage polarization, we cultured *Maoa* WT and KO BMDMs *in vitro* and polarized these macrophages toward an immunosuppressive phenotype by adding anti-inflammatory stimuli (i.e., IL-4 and IL-13; Fig. 3a). We observed a sharp induction of *Maoa* mRNA expression in *Maoa* WT BMDMs during macrophage development, that remained high post-IL-4/IL-13 stimulation (Fig. 3b,c). MAO-A expression was undetectable in *Maoa* KO BMDMs, confirming their *Maoa*-deficiency genotype (Fig. 3b,d). Compared to their wildtype counterpart, *Maoa* KO macrophages displayed a less immunosuppressive phenotype under IL- 4/IL-13 stimulation, evidenced in their reduced expression of immunosuppressive markers (i.e., CD206; Fig. 3e) and signature genes (i.e., *Chi3l3* and *Arg1*; Fig. 3f,g). When tested in a macrophage/T cell co-culture assay (Fig. 3h), in agreement with their less immunosuppressive phenotype, IL-4/IL-13-polarized *Maoa* KO macrophages exhibited impaired suppression of wildtype $CD8^+$ T cells under anti-CD3/CD28 stimulation, shown as their attenuated inhibition of $CD8^+$ T cell proliferation (Fig. 3i) and activation marker expression (i.e., upregulation of CD25 and CD44, and downregulation of CD62L; Fig. 3j,k and Supplementary Fig. 3a).

To verify whether MAO-A deficiency directly contributed to the alleviated immunosuppressive polarization of *Maoa* KO macrophages, we performed a rescue experiment. We constructed a MIG-*Maoa* retroviral vector, used this vector to transduce *Maoa* KO BMDMs, and achieved overexpression of MAO-A in these

macrophages (Fig. 3l-n, and Supplementary Fig. 3b). MAO-A overexpression significantly exacerbated the immunosuppressive phenotype of IL- 4/IL-13-stimulated *Maoa* KO BMDMs (i.e., upregulation of immunosuppressive signature genes such as *Chi3l3* and *Arg1*; Fig. 3o,p). Taken together, these results indicate that MAO-A acts as an autonomous factor promoting macrophage immunosuppressive polarization under anti- inflammatory stimuli.

MAO-A promotes macrophage immunosuppressive polarization via ROS upregulation

Next, we sought to investigate the molecular mechanisms regulating MAO-A promotion of macrophage immunosuppressive polarization. It has been reported that intracellular reactive oxygen species (ROS; hence, oxidative stress) elicit macrophage immunosuppressive features [57, 58, 59, 60, 61]. MAO-A catalyzes the oxidative deamination of monoamines, thereby generating hydrogen peroxide (H_2O_2) as a byproduct that can increase intracellular ROS levels. We therefore speculated that MAO-A might promote TAM immunosuppressive polarization in TME via upregulating ROS levels in TAMs (Fig. 4a).

To test this hypothesis, we directly measured ROS levels in TAMs isolated from *Maoa* WT and KO mice bearing B16-OVA tumours and detected significantly lower levels of ROS in *Maoa* KO TAMs (Fig. 4b,c). Measurement of ROS levels in *in vitro*-cultured *Maoa* WT and KO BMDMs also showed reduced levels of ROS in *Maoa* KO BMDMs, with or without IL-4/IL-13 stimulation, in agreement with the *in vivo* TAM results (Fig. 4d). Supplementing H_2O_2 to IL-4/IL-13-stimulated *Maoa* WT and KO BMDMs elevated their intracellular ROS to similar levels (Supplementary Fig. 4a,b) and eliminated their differences in expression of immunosuppressive markers (i.e., CD206; Fig. 4e) and signature genes (i.e., *Chi3l3* and *Arg1*; Fig. 4f,g).

On the other hand, supplementation of tyramine, a substrate of MAO-A, increased ROS levels and upregulated the expression of immunosuppressive genes (i.e., *Chi3l3* and *Arg1*) in *Maoa* WT BMDMs but not in *Maoa* KO BMDMs (Fig. 4h-j). Taken together, these data indicate that MAO-A regulates macrophage immunosuppressive polarization via modulating macrophage intracellular ROS levels.

The JAK-Stat6 signaling pathway plays a key role in mediating IL-4/IL-13-induced immunosuppressive polarization of TAMs in TME [62, 63]. After IL-4/IL-13 stimulation, JAK is phosphorylated and subsequently phosphorylates Stat6; phosphorylated Stat6 dimerizes and migrates to the nucleus, where it binds to the promoters of IL-4 and IL-13 responsive genes including those involved in macrophage immunosuppressive functions [64, 65]. ROS has been reported to promote JAK and Stat6 phosphorylation in a variety of cell types [61, 66, 67, 68, 69, 70, 71]. Since we observed decreased ROS levels in *Maoa* KO macrophages compared to those in *Maoa* WT macrophages (Fig. 4b,c), we postulated that MAO-A may impact macrophage polarization through upregulating ROS levels and thereby sensitizing the JAK-Stat6 signaling pathway. Indeed, direct analysis of TAMs isolated from B16-OVA tumour-bearing *Maoa* WT and *Maoa* KO mice confirmed that compared to wildtype TAMs, MAO-A-deficient TAMs showed reduced Stat6 activation (i.e., reduced Stat6 phosphorylation; Fig. 4k,l). Further analysis of IL-4/IL-13-induced JAK-Stat6 signaling pathway in *Maoa* KO BMDMs compared to that in *Maoa* WT BMDMs showed significantly

reduced JAK-Stat6 signaling (i.e., reduced JAK1, JAK2, JAK3, and Stat6 phosphorylation; Fig. 4m). Supplementing H_2O_2 to IL-4/IL-13-stimulated *Maoa* WT and KO

BMDMs increased their JAK-Stat6 signaling to similar levels (i.e., comparable JAK1, JAK2, JAK3, and Stat6 phosphorylation; Fig. 4m), corresponding to their comparable high levels of ROS (Supplementary Fig. 4a,b). These data indicate that MAO-A promotes macrophage immunosuppressive polarization via ROS-sensitized JAK-Stat6 pathway activation.

Collectively, these *in vivo* and *in vitro* data support a working model that MAO-A promotes TAM immunosuppressive polarization in TME, at least partly through upregulating TAM intracellular ROS levels and thereby enhancing the IL-4/IL-13-induced JAK-Stat6 signaling pathway.

MAO-A blockade for cancer immunotherapy- syngeneic mouse tumour model studies

The identification of MAO-A as a key regulator of TAM immunosuppressive polarization makes MAO-A a promising new drug target for cancer immunotherapy. Because of the known functions of MAO-A in the brain, small molecule MAOIs have been developed and clinically utilized for treating various neurological disorders, making it a highly feasible and attractive approach to repurpose these established MAOI drugs for cancer immunotherapy [51, 72]. In an *in vitro* WT BMDM IL-4/IL-13-induced polarization culture (Fig. 5a), addition of multiple MAOIs efficiently reduced ROS levels in BMDMs (Fig. 5b) and suppressed their immunosuppressive polarization, evidenced by their decreased expression of immunosuppressive markers (i.e., CD206; Fig. 5c) and immunosuppressive genes (i.e., *Chi3l3* and *Arg1*; Fig. 5d,e). Notably, the MAOIs that we tested include phenelzine, clorgyline, mocolobemide, and pirlindole, covering the major categories of established MAOIs classified on the basis of whether they are nonselective or selective for MAO- A, and whether their effect is reversible (Fig. 5a) [51, 54, 73]. Among these MAOIs, phenelzine (trade name: Nardil) is clinically available in the United States [72]. In the following studies, we chose phenelzine as a representative to study the possibility of repurposing MAOIs for cancer immunotherapy, using two syngeneic mouse tumour models: a B16-OVA melanoma model and a MC38 colon cancer model [74].

First, we studied the therapeutic potential of phenelzine in a B16-OVA tumour prevention model (Fig. 5f). Phenelzine treatment effectively suppressed B16-OVA tumour growth in B6 wildtype mice (Fig. 5g,h). No tumour growth difference was observed when we depleted TAMs in experimental mice via a clodronate liposome treatment, indicating that phenelzine suppressed tumour growth via modulating TAMs (Fig. 5g,h and Supplementary Fig. 5a). Correspondingly, TAMs isolated from phenelzine-treated mice displayed a less immunosuppressive phenotype (i.e., decreased expression of CD206; Fig. 5i) that was correlated with an enhanced antitumour reactivity of tumour-infiltrating $CD8^+$ T cells (i.e., increased production of Granzyme B; Fig. 5j) in these mice. Further studies showed that phenelzine treatment also effectively suppressed the progression of pre-established solid tumours in both B16-OVA and MC38 models (Supplementary Fig. 5b-f).

Next, we evaluated the potential of phenelzine for combination therapy, in particular combining with other ICB therapies such as PD-1/PD-L1 blockade therapy (Fig. 5k). Although most ICB therapies target $CD8^+$ T cells, these cells are in fact closely regulated by TAMs in the TME, making targeting TAMs another potential avenue for immunotherapy [14, 39]. In both B16- OVA and MC38 tumour models, phenelzine treatment significantly suppressed the progression of pre-established solid tumours at a level comparable to the anti-PD-1 treatment; importantly, the combination of phenelzine and anti-PD-1 treatments yielded synergistic tumour suppression efficacy (Fig. 5l-o). These tumour suppression effects of phenelzine were due to immunomodulation but not direct tumour inhibition, because phenelzine treatment did not suppress the growth of B16-OVA and MC38 tumours in immunodeficient NSG mice (Supplementary Fig. 5g-k).

Collectively, these syngeneic mouse tumour model studies provided proof-of-principle evidence for the cancer immunotherapy potential of MAOIs via targeting TAM reprogramming and thereby enhancing antitumour T cell responses.

MAO-A blockade for cancer immunotherapy- human TAM and clinical data correlation studies

To explore the translational potential of MAO-A blockade therapy, we first studied MAO-A regulation of human macrophage polarization. Using a Tumour Immune Dysfunction and Exclusion (TIDE) computational method [75], we analyzed the gene expression signatures of *in vitro* cultured immunostimulatory M1-like and immunosuppressive M2-like human monocyte-derived macrophages (MDMs) (GSE35449) [76]. Interestingly, among all immune checkpoint and immune suppressive genes examined, *MAOA* ranked as the top gene with the most dramatically elevated expression in M2-like MDMs (i.e., 7.28 M2/M1 log-fold change; Fig. 6a), suggesting a possible role of MAO-A in promoting human macrophage immunosuppressive polarization. Time-course analysis of MDM culture confirmed an upregulation of MAO-A gene and protein expression during macrophage differentiation that was further upregulated post IL-4/IL-13-induced immunosuppressive polarization (Fig. 6b-d). Blockade of MAO-A using phenelzine significantly inhibited IL-4/IL-13-induced immunosuppressive polarization of MDMs, evidenced by their decreased expression of immunosuppressive markers (i.e., CD206 and CD273; Fig. 6e and Supplementary Fig. 6a) and signature genes (i.e., *ALOX15* and *CD200R1*; Fig. 6f,g). Collectively, these *in vitro* data suggest that MAO-A is highly expressed in human macrophagesespecially during their immunosuppressive polarization, and that MAO-A blockade has the potential to reprogram human macrophage polarization.

To directly evaluate whether MAO-A blockade could reprogram human TAM polarization *in vivo*, we established a human tumour/TAM xenograft NSG mouse model. A375 human melanoma cells were mixed with monocytes sorted from healthy donor peripheral blood mononuclear cells (PBMCs), and s.c. injected into NSG mice to form solid tumours, with or without phenelzine treatment after inoculation (Fig. 6h). Phenelzine treatment effectively suppressed immunosuppressive polarization of human TAMs (gated as $hCD45^+hCD11b^+hCD14^+$; Supplementary Fig. 6b), supported by their decreased expression of immunosuppressive markers (i.e., CD206 and CD273; Fig. 6i,j).

Next, we studied whether MAO-A blockade-induced human TAM reprogramming could impact human T cell antitumour reactivity, using a 3D human tumour/TAM/T cell organoid culture (Fig. 6k). NY-ESO-1, a well-recognized tumour antigen commonly expressed in a large variety of human cancers [77], was chosen as the model tumour antigen. An A375 human melanoma cell line was engineered to co-express NY-ESO-1 as well as its matching MHC molecule, HLA-A2, to serve as the human tumour target (denoted as A375-A2-ESO; Supplementary Fig. 6c,d). NY-ESO- 1-specific human $CD8^+$ T cells were generated by transducing healthy donor peripheral blood $CD8^+$ T cells with a Retro/ESO-TCR retroviral vector encoding an NY-ESO-1 specific TCR (clone 3A1; denoted as ESO-TCR); the resulting T cells, denoted as ESO-T cells, expressed ESO-TCRs and specifically targeted A375-A2-ESO tumour cells, thereby modeling the tumour-specific human $CD8^+$ T cells (Supplementary Fig. 6e,f). Human MDMs were cultured from healthy donor PBMCs, followed by IL-4/IL-13 stimulation to induce immunosuppressive polarization in the presence or absence of phenelzine treatment (Fig. 6k). The A375-A2-ESO human melanoma cells,ESO-T cells, and IL-4/IL-13-polarized MDMs were mixed at a 2:2:1 ratio and placed in a 3D tumour organoid culture mimicking TME (Fig. 6k). IL-4/IL-13-polarized MDMs effectively suppressed ESO-T cell-mediated killing of A375-A2-ESO tumour cells; this immunosuppressive effect was largely alleviated by phenelzine treatment during MDM polarization (Fig. 6l). Accordingly, ESO-T cells co-cultured with phenelzine-treated MDMs, compared to those co- cultured with non-phenelzine-treated MDMs, showed an enhancement in T cell activation (i.e., increased cell number, increased CD25 expression, and decreased CD62L expression; Fig. 6m and Supplementary Fig. 6g). Collectively, these data suggest that MAO-A blockade-induced human TAM reprogramming has the potential to improve antitumour T cell responses.

To study *MAOA* gene expression in primary human TAMs, we collected fresh ovarian cancer tumour samples from patients, isolated TAMs (sorted as $DAPI^-hCD45^+hCD11b^+hTCR\alpha\beta^-hCD14^+$ cells; Supplementary Fig. 6h), and assessed their *MAOA* gene expression. Primary human monocytes isolated from health donor PBMCs (sorted as $DAPI^-hCD45^+hCD11b^+hTCR\alpha\beta^-hCD14^+$ cells; Supplementary Fig. 6i) were included as controls. Like mouse TAMs, human TAMs expressed high levels of *MAOA* gene, confirming MAO-A as a valid drug target in human TAMs (Fig. 1a and Fig. 6n).

Lastly, we conducted clinical data correlation studies to investigate whether intratumoural *MAOA* gene expression is correlated with clinical outcomes in cancer patients, using the TIDE computational method Intratumoural *MAOA* expression level was negatively correlated with patient survival in multiple cancer patient cohorts spanning ovarian cancer (Fig. 6o) [78], lymphoma (Fig. 6p) [79], and breast cancer (Fig. 6q) [80]. Moreover, analysis of a melanoma patient cohort receiving anti-PD-1 treatment showed that high levels of intratumoural *MAOA* expression largely abrogated the survival benefit offered by the PD-1 treatment, suggesting that combining MAO-A blockade therapy with PD-1/PD-L1 blockade therapy may provide synergistic therapeutic benefits through modulating TAM polarization and thereby changing the immunosuppressive TME and improving antitumour immunity (Fig. 6r) [81]. Of note, these whole tumour lysate transcriptome data analyses could not localize the *MAOA* expression to a specific cell type (e.g., TAMs); future studies of quality transcriptome data generated from single cells or sorted TAMs are needed to obtain such information. Nonetheless, the present clinical data correlation studies identified

MAO-A as a possible negative regulator of survival in a broad range of cancer patients, including those receiving existing ICB therapies, suggesting MAO-A blockade as a promising avenue for developing new forms cancer therapy and combination therapy.

Taken together, these human TAM and clinical correlation studies confirmed MAO-A as a promising drug target in human TAMs and support the translational potential of MAO-A blockade for cancer immunotherapy through targeting TAM reprogramming.

Discussion

Based on our findings, we propose an “intratumoural MAO-A-ROS axis” model to elucidate the role of MAO-A in regulating TAM immunosuppressive polarization (Supplementary Fig. 7). Analogous to the well-characterized MAO-A-ROS axis in the brain, where MAO-A controls ROS levels in neurons and thereby modulates neuron degeneration via regulating neuron oxidative stress, the MAO-A-ROS axis in a solid tumour controls ROS levels in TAMs and thereby modulates TAM immunosuppressive polarization via sensitizing the IL-4/IL-13-induced JAK- Stat6 signaling pathway (Supplementary Fig. 7). The resemblance between these mechanisms is intriguing: from an evolutionary point of view, it makes sense that some critical molecular regulatory pathways are preserved between the nervous and immune systems, considering that both systems are evolved to defend a living organism by sensing and reacting to environmental danger and stress. Indeed, neurons and immune cells share a broad collection of surface receptors, secretory molecules, and signal transducers [82]. In particular, many neurotransmitters/neuropeptides and their synthesis/degradation machineries traditionally considered specific for neurons are expressed in immune cells, although their functions in the immune system are to a large extent still unknown [83, 84]. Studying these molecules and their regulatory mechanisms may provide new perspectives in tumour immunology and identifying new drug targets for cancer immunotherapies, as exemplified by our current finding of this “MAO-A-ROS axis” regulation of TAM polarization in the TME.

Considering the importance of TAMs in regulating antitumour immunity, there has been considerable efforts in developing cancer therapeutic strategies targeting TAMs. These strategies can be roughly divided into two categories: 1) those which deplete TAMs, and 2) those which alter TAM immunosuppressive activities [39]. The first category includes strategies targeting TAM recruitment and survival, such as blocking the CCL2-CCR2 axis thereby preventing monocyte mobilization from the bone marrow and recruitment into inflammatory sites, or blocking the CSF1- CSF1R axis thereby inducing apoptosis of TAMs, or blocking the CXCL12-CXCR4 and angiopoietin 2 (ANG2)-TIE2 axes thereby depleting $TIE2^{+}$ macrophages that are critical for tumour angiogenesis [19, 39, 85]. However, an intrinsic downside of depleting TAMs is the loss of their innate immunostimulatory role as the primary phagocytes and professional antigen-presenting cells (APCs) in solid tumours. Reprogramming or repolarizing immunosuppressive TAMs towards an immunostimulatory phenotype therefore can be an attractive direction; this second category of TAM-repolarizing strategies includes those reprogramming TAMs via

CD40 agonists, HDAC inhibitors, PI3K*g* inhibitors, and creatine [39, 40, 86, 87, 88]. Many of these TAM reprogramming strategies are currently under active clinical evaluation [39]. Notably, CD40 agonists work through activating CD40L-downstream NF-kB pathway [87, 89]; HDAC inhibitors work through altering histone modifications [86, 90, 91]; PI3Kγ inhibitors work through stimulating NF-κB activation while inhibiting C/EBPβ activation [88, 92, 93]; and creatine uptake works through regulating cytokine responses [40]. Our discovery of MAO-A as a critical regulator of TAM polarization through modulating oxidative stress provides a new drug target and a new mechanism of action (MOA) for expanding TAM-repolarizing strategies.

Compared to many new therapeutic candidates, MAO-A is unique in that it is already an established drug target due to its known functions in the brain [72]. In fact, small molecule MAOIs have been developed to block MAO-A enzymatic activity in the brain and are clinically used for treating various neurological disorders [72]. Notably, some MAOIs cross-inhibit the MAO-A isoenzyme MAO-B, that co-expresses with MAO-A in the brain (Supplementary Fig. 7) [51]. However, in human macrophages, especially in M2-like immunosuppressive macrophages, MAO- A is the dominant form (i.e., the expression of *MAOA* was about 40-fold higher than that of *MAOB* in M2-like human macrophages; Supplementary Fig. 8) [76]. In our studies, we tested multiple clinically approved MAOIs (phenelzine, clorgyline, moclobemide, and pirlindole) and demonstrated their efficacy in regulating macrophage ROS levels and immunosuppressive polarization, pointing to the possibility of repurposing these drugs for cancer immunotherapy (Fig. 5 and 6). Developing new cancer drugs is extremely costly and time-consuming; drug repurposing offers an economic and speedy pathway to novel cancer therapies because approved drugs have known safety profiles and modes of actions and thus can enter the clinic quickly [94].

MAOIs had been used extensively over two decades after their introduction in the 1950s, but since then their use has declined because of reported side effects and the introduction of other classes of antidepressant drugs [72]. However, these MAOIs side effects were vastly overstated and should be revisited [72]. For instance, a claimed major side effect of MAOIs is the risk of triggering tyramine-induced hypertensive crisis when patients eat tyramine-rich foods such as aged cheese (hence, “cheese effects”); this concern led to cumbersome food restrictions that are now considered largely unnecessary [72]. A transdermal delivery system (Emsam) has also been developed to deliver MAOIs that can largely avoid potential food restrictions [95]. Therefore, interest in MAOIs as a major class of antidepressants is reviving, and repurposing MAOIs for cancer immunotherapy can be an attractive new application of these potent drugs [72]. Moreover, many cancer patients suffer from depression and anxiety; these overwhelming emotional changes can negatively interfere with the quality of life and cancer treatment efficacy of cancer patients [96]. Repurposing MAOIs for cancer immunotherapy thus may provide cancer patients with anti-depression and antitumour dual benefits, making this therapeutic strategy particularly attractive.

Because preclinical evidence largely supports combinatorial approaches being necessary to achieve significant antitumour efficacy, most TAM-targeting strategies currently under clinical evaluation are tested in combination with standard chemotherapy or radiation therapy, or in combination with T cell-

directed ICB therapies such as PD-1 or/and PD-L1 blockade therapy [39]. In our study, we found that MAOI treatment synergized with anti-PD-1 treatment in suppressing syngeneic mouse tumour growth (Fig. 5k-o), and that intratumoural *MAOA* gene expression levels dictated poor patient survival in melanoma patients receiving anti-PD-1 therapy (Fig. 6r). These data highlight the promise of MAOI treatment as a valuable component for combination cancer therapies.

In summary, here we identified MAO-A as a critical molecule regulating TAM immunosuppressive polarization and thereby modulating antitumour immunity, and demonstrated the potential of repurposing established MAOI antidepressants for cancer immunotherapy. Future clinical studies are encouraged to investigate the clinical correlations between MAOI treatment and clinical outcomes in cancer patients and to explore the possibility of repurposing MAOIs for combination cancer therapies. Meanwhile, the immune regulatory function of MAO-A certainly goes beyond regulating TAM polarization. In *Maoa* KO mice, we have observed the changes of antitumour responses of multiple immune cells in various syngeneic mouse tumour models. It is also likely that MAO-A regulates immune reactions to other diseases such as infection diseases and autoimmune diseases. Studying the roles of MAO-A in regulating various immune cells under different health and disease conditions will be interesting topics for future research.

Methods

Mice

C57BL/6J (B6), B6.SJL-*Ptprc*^{a} *Pepc*$^{b/}$BoyJ (CD45.1, BoyJ), 129S-*Maoa*$^{tm1Shih/}$J (*Maoa* KO) [56], and NOD.Cg-*Prkdc*^{scid} *Il2rg*$^{tm1Wjl/}$SzJ (NSG) mice were purchased from the Jackson Laboratory (Bar Harbor). *Maoa* KO mice were backcrossed with C57BL/6J mice for more than 9 generations at the University of California, Los Angeles (UCLA). Eight- to twelve-week-old female mice were used for all experiments unless otherwise indicated. Due to ethical reasons, we ended experiments before tumour volume surpassed 1000 mm^3. All mice experiments were repeated at least three times unless specifically mentioned. Replicates of each individual experiment was stated in its figure legends. All animals were maintained at the UCLA animal facilities and all animal experiments were approved by the Institutional Animal Care and Use Committee of UCLA.

Human tumour samples

All human samples were obtained following institutional guidelines under protocols approved by the institutional review boards (IRBs) at the UCLA Medical Center. Primary human ovarian cancer tumour samples were obtained from the operating room at the UCLA Medical Center from consenting patients using IRB-approved protocols (IRB# 10–000727). Tumours specimens were brought back to the laboratory for further analyses. Detailed patients information is provided in Supplementary Table 1, including collection date, age, diagnosis and staging.

Cell lines and viral vectors

The B16-OVA mouse melanoma cell line and the PG13 retroviral packaging cell line were provided by Dr. Pin Wang (University of South California, CA) [97]. The MC–38 mouse colon adenocarcinoma cell line was provided by Dr. Antoni Ribas (UCLA) [74]. The HEK 293T and Phoenix-ECO retroviral packaging cell lines, the A375 human melanoma cell line, and the L–929 mouse connective tissue cell line were purchased from the American Type Culture Collection (ATCC). The A375-A2-ESO cell line was previously reported [98]. The Phoenix-ECO-MIG, Phoenix-ECO-MIG-*Maoa,* and PG13-ESO-TCR stable virus producing cell lines were generated in this study. The MIG (MSCV-IRES-GFP) retroviral vector was reported previously [99, 100, 101]. MIG-*Maoa* and Retro/ESO-TCR retroviral vectors were generated in this study.

Syngeneic mouse tumour models

B16-OVA melanoma cells (1 x 10^6 per animal) or MC38 colon cancer cells (5 x 10^5 per animal) were subcutaneously (s.c.*)* injected into experimental mice to form solid tumours. In some experiments, mice received intraperitoneal (i.p.*)* injection of phenelzine (30 mg/kg/day) to block MAO-A activity. In some experiments, mice received i.p. injection of clodronate liposomes (200 µl/animal, twice per week) to deplete TAMs; mice received i.p. injection of vehicle liposomes (200 µl/animal, twice per week) were included as controls. In some experiments, mice received i.p. injection of anti-mouse PD–1 antibodies (300 µg/animal, twice per week) to block PD–1; mice received i.p. injection of isotype antibodies were included as controls. During an experiment, tumour growth was monitored twice per week by measuring tumour size using a Fisherbrand™ Traceable™ digital caliper (Thermo Fisher Scientific); tumour volumes were calculated by formula 1/2 x L x W^2. At the end of an experiment, solid tumours were collected and tumour- infiltrating immune cells were isolated for analysis using QPCR, flow cytometry, and/or scRNASeq.

Bone marrow (BM) transfer mouse tumour model

BM cells were collected from femurs and tibias of *Maoa* WT and *Maoa* KO donor mice, and were separately transferred into BoyJ (CD45.1) wildtype recipient mice that were preconditioned with whole body irradiation (1,200 rads). Recipient mice were maintained on antibiotic water (Amoxil, 0.25 mg/ml) for 4 weeks after BM transplantation. Periodical bleedings were performed to monitor immune cell reconstitution using flow cytometry. Tumour inoculation started at 12 weeks post BM transfer when recipient mice were fully immune reconstituted. B16-OVA mouse melanoma cells were s.c. injected into recipient mice to form solid tumours (1 x 10^6 cells per animal). Tumour growth was monitored twice per week by measuring tumour size using a Fisherbrand™ Traceable™ digital caliper; tumour volumes were calculated by formula 1/2 x L x W2. At the end of an experiment, tumour-infiltrating immune cells were isolated for analysis using flow cytometry.

Syngeneic mouse tumour-TAM co-inoculation model

Bone marrow cells were collected from *Maoa* WT and *Maoa* KO mice and were cultured *in vitro* to generate bone marrow-derived macrophages (BMDMs). B16-OVA tumour cells (1 x 10^6 cells per mouse) and BMDMs (5 x 10^6 cells per mouse) were mixed and s.c. injected into BoyJ mice to form solid tumours. Tumour growth was monitored twice per week by measuring tumour size using a Fisherbrand™ Traceable™ digital caliper; tumour volumes were calculated by formula 1/2 x L x W^2.At the end of an experiment, tumours were collected and tumour-infiltrating immune cells were isolated for analysis using flow cytometry.

Xenograft human tumour-TAM co-inoculation model

Human peripheral blood mononuclear cells (PBMCs) of healthy donors were obtained from the CFAR Gene and Cellular Therapy Core Laboratory at UCLA, without identification information under federal and state regulations. Human monocytes were isolated from healthy donor PBMCs via magnetic-activated cell sorting (MACS) using human CD14 microbeads (Miltenyi Biotec, 130–050–201)followedbyfluorescenceactivatedcellsorting(FACS;sorted as $hCD45^+hCD11b^+hCD14^+$ cells) using a FACSAria II flow cytometer (BD Biosciences). Human A375 melanoma cells (10 x 10^6 cells per animal) and purified human monocytes (5 x 10^6 cells per animal) were mixed and s.c. injected into NSG mice to form solid tumours. Some experimental animals received i.p. injection of MAOI (phenelzine, 30 mg/kg/day) to block MAO-A activity. At the end of an experiment, tumour-associated immune cells were isolated foranalysis using flow cytometry.

Tumour-infiltrating immune cell (TII) isolation and analysis

Solid tumours were collected from experimental mice at the termination of a tumour experiment. Tumours were cut into small pieces and smashed against a 70-μm cell strainer (Corning, 07–201- 431) to prepare single cells. Immune cells were enriched through gradient centrifugation with 45% Percoll (Sigma-Aldrich, P4937) at 800 g for 30 mins at 25 °C without braking, followed by treatment with Tris-buffered ammonium chloride buffer to lyse red blood cells according to a standard protocol (Cold Spring Harbor Protocols). The resulting TII isolates were then used for further analysis.

In some experiments, TII isolates were sorted via FACS using a FACSAria II flow cytometer (BD Biosciences) to purify TAMs (sorted as $DAPI^-CD45.2^+CD11b^+Ly6G^-Ly6C^-/lowF4/80^+$ cells), which were then subjected to QPCR analysis of *Maoa* mRNA expression in TAMs.

In some experiments, TII isolates were sorted via FACS using a FACSAria II flow cytometer (BD Biosciences) to purify immune cells (sorted as $DAPI^-CD45.2^+$ cells), which were then subjected to scRNASeq analysis of gene expression profiling of TIIs.

In some experiments, TIl isolates were directly analyzed using MACSQuant Analyzer 10 Flow Cytometer (Miltenyi Biotec) to study the cell surface marker expression of TAMs (pre-gated as $CD45.2^+CD11b^+Ly6G^-Ly6C^{-/low}F4/80^+$ cells) and the intracellular effector molecule production of $CD8^+$ T cells (pre-gated as $CD45.2^+TCR\beta^+CD8^+$ cells).

Mouse bone marrow-derived macrophages (BMDM) culture and polarization

To generate BMDMs, BM cells were collected from femurs and tibias of *Maoa*WT mice and *Maoa* KO mice, and were cultured in C10 medium containing with 20% of L929-conditional medium in a 10-cm dish (2×10^6 cells per ml; 12 ml per dish) for 6 days. At day 6, the resulting BMDMs were collected and reseeded in a 6-well plate (1×10^6 cells per ml; 2 ml per well) in C10 medium for 24 hours, in the presence or absence of recombinant murine IL–4 (10 ng/ml) (Peprotech, 200–04) and IL–13 (10 ng/ml) (Peprotech, 200–13) to induce BMDM immunosuppressive polarization.

In some experiments, MAOIs were added to the *Maoa* WT BMDM polarization culture 30 minutes prior to adding recombinant murine IL–4 and IL–13, to block MAO-A activity during BMDM polarization. MAOIs studied were phenelzine (Phe, 20 μM) (Sigma-Aldrich), clorgyline (Clo, 20 μM) (Sigma-Aldrich), moclobemide (Moc, 200 μM) (Sigma-Aldrich), and pirlindole (Pir, 20 μM) (R&D Systems). At 24 hours after IL–4/IL–13 stimulation, BMDMs were collected for analysis.

In some experiments, H_2O_2 (100 μM) were added to the *Maoa*WT and *Maoa* KO BMDM polarization culture 30 minutes prior to adding recombinant murine IL–4 and IL–13. At 30 minutes after IL–4/IL–13 stimulation, BMDMs were collected for WB analysis; at 24 hours after IL–4/IL- 13 stimulation, BMDMs were collected for flow cytometry and QPCR analysis.

In some experiments, tyramine (100 μM) (Sigma-Aldrich, T90344) were added to the *Maoa*WT and *Maoa* KO BMDM polarization culture 30 minutes prior to adding recombinant murine IL–4 and IL–13. At 24 hours after IL–4/IL–13 stimulation, BMDMs were collected for flow cytometry and QPCR analysis.

Macrophage suppressive function assay

IL–4/IL–13 polarized *Maoa* WT and *Maoa* KO BMDMs were mixed with splenocytes harvested from B6 wildtype mice at 0:1, 1:2, 1:4, or 1:8 ratio, then cultured in a 24-well plate in C10 medium (1×10^6 splenocytes/ml/well), in the presence of plate-bound anti-mouse CD3ε (5 μg/ml) and soluble anti-mouse CD28 (1 μg/ml) for 2 days. At the end of a culture, cells were collected for flow cytometry analysis.

MIG-Maoa retroviral vector construction, production, and macrophage transduction

MIG retroviral vector was reported previously [99, 100, 101]. Codon-optimized *Maoa* cDNA (synthesized by IDT) was inserted into a MIG retroviral vector to generate the MIG-*Maoa* retroviral vector. Vsv-g-pseudotyped MIG and MIG-Maoa retroviruses were produced using HEK 293T virus packaging cells following a standard calcium precipitation method [100, 101], and then were used to transduce Phoenix-ECO cells to generate stable cell lines producing ECO- pseudotyped MIG or MIG-*Maoa* retroviruses (denoted as Phoenix-ECO-MIG and Phoenix-ECO- MIG-*Maoa* cell lines, respectively). For virus production, Phoenix-ECO-MIG and Phoenix-ECO- MIG-*Maoa* cells were seeded at a density of 0.8 x 10^6 cells per ml in D10 medium, and cultured in a 15-cm dish (30 ml per dish) for 2 days. Virus supernatants were then collected and used for macrophage transduction.

BM cells harvested from *Maoa* WT and *Maoa* KO mice were cultured in a 6-well plate in C10 medium containing 20% L929-conditional medium (4 x 10^6 cells/2 ml/well) for 6 days, to differentiate into BMDMs. From day 1 to day 5, cells were spin-infected daily with virus supernatants supplemented with polybrene (10 μg/ml) at 660 g at 30 °C for 90 minutes. At day 6, recombinant murine IL–4 (10 ng/ml) and IL–13 (10 ng/ml) were added to cell culture to induce BMDM immunosuppressive polarization. At day 7, transduced BMDMs were collected for flow cytometry analysis of transduction efficiency (%GFP^+ cells of total cells); GFP^+ BMDMs were sorted via FACS using a FACSAria II flow cytometer (BD Biosciences) and were then used for QPCR analysis of immunosuppressive gene expression.

Human monocyte-derived macrophage (MDM) culture and polarization

Human peripheral blood mononuclear cells (PBMCs) of healthy donors were obtained from the CFAR Gene and Cellular Therapy Core Laboratory at UCLA, without identification information under federal and state regulations. Human monocytes were isolated from healthy donor PBMCs by adherence. Briefly, PBMCs were suspended in serum-free RPMI 1640 media (Corning Cellgro, 10–040-CV) at 10 x 10^6 cells/ml. 12.5 ml of the cell suspension were added to each 10-cm dish and incubated for one hour in a humidified 37°C, 5% CO_2 incubator. Medium that contained non- adherent cells was discarded. Dishes were washed twice and adherent monocytes were cultured in C10 media with human M-CSF (10 ng/ml) (Peprotech, 300–25) for 6 days to generate MDMs. At day 6, the resulting MDMs were collected and reseeded in a 6-well plate in C10 medium (1 x 10^6 cells/ 2 ml/well) for 48 hours, in the presence or absence of recombinant human IL–4 (10 ng/ml) (Peprotech, 214–14) and human IL–13 (10 ng/ml) (Peprotech, 214–13) to induce MDM immunosuppressive polarization. In some experiments, MAOIs (phenelzine, 20 μM) were added to the MDM polarization culture 30 minutes prior to adding recombinant human IL–4 and human IL–13, to block MAO-A activity during MDM polarization. Polarized MDMs were then collected and used for flow cytometry and QPCR analysis or for setting up the 3D human tumour organoid culture experiments.

Human NY-ESO–1-specific TCR-engineered CD8+ T (ESO-T) cells

The Retro/ESO-TCR vector was constructed by inserting into the parental pMSGV vector a synthetic gene encoding an HLA-A2-restricted, NY-ESO–1 tumour antigen-specific human CD8 TCR (clone 3A1) [98]. Vsv-g-pseudotyped Retro/ESO-TCR retroviruses were generated by transfecting HEK 293T cells following a standard calcium precipitation protocol and an ultracentrifugation concentration protocol [102]; the viruses were then used to transduce PG13 cells to generate a stable retroviral packaging cell line producing GALV-pseudotyped Retro/ESO-TCR retroviruses (denoted as the PG13-ESO-TCR cell line). For virus production, the PG13-ESO-TCR cells were seeded at a density of 0.8 x 10^6 cells per ml in D10 medium, and cultured in a 15-cm dish (30 ml per dish) for 2 days; virus supernatants were then harvested and stored at –80 °C for future use.

Healthy donor PBMCs were cultured in a 12-well plate in C10 medium (1 x 10^6 cells/ml/well) for 2 days, stimulated with Dynabeads™ Human T-Activator CD3/CD28 (10 µl/ml) (GIBCO, 11161D) and recombinant human IL–2 (20 ng/ml) (Peprotech). After 2 days, dynabeads were removed and cells were spin-infected with frozen-thawed Retro/ESO-TCR retroviral supernatants supplemented with polybrene (10 µg/ml) at 660 g at 30 °C for 90 minutes following an established protocol [98]. Transduced human $CD8^+$ T cells (denoted as ESO-T cells) were expanded for another 6–8 days in C10 medium containing recombinant human IL–2 (20 ng/ml) (Peprotech), and then cryopreserved for future use. Mock-transduced human $CD8^+$ T cells (denoted as Mock-T cells) were generated as controls.

3D human tumour/TAM/T cell organoid culture

A375-A2-ESO human melanoma cell line was generated by engineering the parental A375 cell line to overexpress an NY-ESO–1 tumour antigen as well as its matching HLA-A2 molecule [98].

Human MDMs were generated from healthy donor PBMCs and polarized with IL–4/IL–13 in the presence or absence of phenelzine treatment. ESO-T cells were generated by engineering healthy donor PBMC $CD8^+$ T cells to express an NY-ESO–1-specific TCR (clone 3A1). The A375-A2-ESO tumour cells, MDMs, and ESO-T cells were mixed at a 2:1:2 ratio. Mixed cells were centrifuged and resuspended in C10 medium at 1 x 10^5 cells per µl medium. The cell slurry was >adjusted to 5 ul per aggregate and was gently transferred onto a microporous membrane cell insert (Millicell, PICM0RG50) using a 20-µl pipet to form a 3D human tumour/TAM/T cell organoid. Prior to cell transfer, cell inserts were placed in a 6-well plate immersed with 1 ml C10 medium. Two days later, the organoids were dissociated by P1000 pipet tip and disrupted through a 70-µm nylon strainer to generate single cell suspensions for further analysis.

Reagents

Adherent cell line culture medium (denoted as D10 medium) was made of Dulbecco's modified Eagle's medium (DMEM, Corning Cellgro, 10–013-CV) supplemented with 10% fetal bovine serum (FBS, Sigma-Aldrich, F2442) and 1% Penicillin-Streptomycin-Glutamine (Gibco, 10378016). T cell and macrophage culture medium (denoted as C10 medium) was made of RPMI 1640 (Corning Cellgro, 10–040-CV) supplemented with 10% FBS (Sigma-Aldrich), 1% Penicillin- Streptomycin-Glutamine (Gibco), 0.2% Normocin (Invivogen, ant-nr–2), 1% MEM Non-Essential Amino Acids Solution (Gibco, 11140050), 1% HEPES (Gibco, 15630056), and 1% Sodium Pyruvate (Gibco, 11360070).

Macrophage culture reagents, including recombinant murine IL–4, recombinant murine IL- 13, recombinant human M-CSF, recombinant human IL–4, and recombinant human IL–13 were purchased from PeproTech. T cell culture reagents, including purified NA/LE anti-mouse CD3ε (clone 145–2C11), anti-mouse CD28 (clone 37.51), anti-human CD3 (clone OKT3), and anti- human CD28 (clone CD28.2), were purchased from BD Biosciences. Recombinant human IL–2 was purchased from PeproTech. Hydrogen peroxide solution was purchased from Sigma-Aldrich (216763).

In vivo PD–1 blocking antibody (clone RMP1–14) and its isotype control (rat IgG2a) were purchased from BioXCell. *In vivo* TAM depletion clodronate liposomes and their control vehicle liposomes were purchased from Clodrosome.

Monoamine oxidase inhibitors (MAOIs), including phenelzine, moclobimide, and clorgyline, were purchased from Sigma-Aldrich. Pirlindole was purchased from R&D systems.

Detailed reagent information is provided in Supplementary Table 2.

Flow cytometry

Flow cytometry, also known as FACS (fluorescence-activated cell sorting), was used to analyze surface marker and intracellular effector molecule expression in immune cells. Fluorochrome- conjugated monoclonal antibodies specific for mouse CD45.2 (clone 104), CD11b (Clone M1/70), Ly6G (Clone 1A8), F4/80 (Clone BM8), Ly6C (Clone HK1.4), CD206 (Clone C068C2), CD69 (clone H1.2F3), CD86 (Clone GL–1), I-Ab (Clone AF6–120.1), TCRβ (clone H57–597), CD45.1

(Clone A20), CD4 (Clone GK1.5), CD8 (clone 53–6.7), CD25 (clone PC61), CD44 (clone IM7), CD62L (clone MEL–14), and Granzyme B (Clone QA16A02) were purchased from BioLegend. Mouse Fc Block (anti-mouse CD16/32; clone 2.4G2) was purchased from BD Biosciences. Fluorochrome-conjugated monoclonal antibodies specific for human CD45 (clone H130), CD11b (Clone ICRF44), CD14 (Clone HCD14), CD206 (Clone 15–2), CD273 (Clone 24F.10C12), TCR*αβ*(clone I26), CD4 (clone OKT4), CD8 (clone SK1), CD44 (clone IM7), CD62L (clone DREG–56), and human Fc Receptor Blocking Solution (TruStain FcX™, 422302) were purchased from BioLegend. Fixable Viability Dye eFluor 506 was purchased from Thermo Fisher Scientific. DAPI (Thermo Fisher Scientific) was included to exclude dead cells in FACS sorting.

To study cell surface marker expression, cells were stained with Fixable Viability Dye followed by Fc blocking and surface marker staining, following a standard procedure as described previously [101]. To study T cell intracellular cytotoxicity molecule production, intracellular staining of Granzyme B was performed using the BD Cytofix/CytopermTM Fixation/Permeabilization Kit (BD Biosciences, 55474) following the manufacturer's instructions. These cells were co-stained with surface markers to identify $CD8^+$ T cells (gated as $TCR\beta^+CD8^+$ cells *in vitro* or $CD45.2^+TCR\beta^+CD8^+$ cells *in vivo)*..

Stained cells were analyzed using a MACSQuant Analyzer 10 flow cytometer (Miltenyi Biotec); data were analyzed using a FlowJo software (BD Biosciences).

Detailed reagent and resources information is provided in Supplementary Table 2.

Western blot (WB)

Total protein was extracted using a RIPA lysis buffer (PIERCE, Roche, Thermo Fisher Scientific) supplemented with protease inhibitor cocktail cOmplete Mini (1 tablet/10 ml) (Sigma-Aldrich, 4693159001) and phosphotase inhibitor PhosSTOP (1 tablet/10 ml) (Sigma-Aldrich, 4906845001), then transferred to pre-cooled eppendorf tubes. The lysed solution was kept on ice for 30 minutes, and then centrifuged at 15,000 g for 5 minutes at 4°C. Supernatants were collected and protein concentrations were quantified using a BCA protein assay (PIERCE, Thermo Fisher Scientific, 23225). Equal amounts of protein were loaded and separated by 8% sodium dodecyl sulfate- polyacrylamide gel electrophoresis (SDS-PAGE), and then transferred to an Immunobilon-P PVDF Membrane (Millipore). The membranes were blocked with a SuperBlock™ T20 (TBS) Blocking Buffer (Thermo Fisher Scientific, 37536). Antibodies were diluted in 5% nonfat milk dissolved in washing buffer TBST (20 mM Tris–HCl, 150 mM NaCl, 0.1% Tween–20).

Primary antibodies against mouse Stat6, p-Stat6 (Tyr641), JAK1, p-JAK1 (Tyr1034/1035), JAK2, p-JAK2 (Tyr1008), JAK3, p-JAK3 (Tyr980/981), HRP-labeled anti-rabbit secondary antibodies, and HRP-labeled anti-mouse secondary antibodies were purchased from Cell Signaling Technology. MAO-A antibody was purchased from Abcam (Clone EPR7101). Primary antibodies against ⍺-actin (Santa Cruz Biotechnology) were used as an internal control for total protein extracts. Signals were visualized using a ChemiDoc Image System (Bio-Rad). Data were analyzed using an Image J software (Bio-Rad).

Detailed reagent information is provided in Supplementary Table 2.

Quantitative real-time PCR (QPCR)

Total RNA was extracted from cells using TRIzol reagent (Invitrogen, Thermo Fisher Scientific, 15596018) following the manufacturer's instructions. SuperScript III First-strand (Thermo Fisher Scientific, 18080051) was used for reverse transcription. QPCR was performed using a KAPA SYBR FAST qPCR

Master Mix (Kapa Biosystems) and a 7500 Real-time PCR System (Applied Biosystems) according to the manufacturers' instructions. Housekeeping gene *Ube2d2* was used as an internal control for mouse immune cells and *ACTB* was used as an internal control for human immune cells. The relative expression of a target gene was calculated using the ΔΔCT method. All primers used in this study are listed in Supplementary Table 3.

Reactive oxygen species (ROS) measurement

Cells were stained with surface marker antibodies, washed with PBS, then resuspended in pre- warmed PBS (1 x 10^6 cells/ml/tube) containing 1 μM CM-H2DCFDA (Thermo Fisher Scientific, C6827). After 15 minutes incubation at room temperature, cells were immediately washed with cold PBS followed by flow cytometry analysis. ROS levels were measured by oxidation of the CM-H2DCFDA probes that can be read out as the fluorescence intensity at the FITC/488 channel of a flow cytometer.

Single cell RNA sequencing (scRNAseq)

scRNASeq was used to analyze the gene expression profiles of TIIs. B16-OVA tumours were harvested from *Maoa* WT and *Maoa* KO mice to prepare TII suspensions (10 tumours were combined for each group). TII suspensions were then sorted using a FACSAria II flow cytometer to purify immune cells (gated as $DAPI^-CD45.2^+$ cells). Sorted TIIs were immediately delivered to the Technology Center for Genomics & Bioinformatics (TCGB) facility at UCLA for library construction and sequencing. Cells were stained with trypan blue (Thermo Fisher Scientific, T10282) and counted using a Cell Countess II automated cell counter (Thermo Fisher Scientific).

10,000 TIIs from each experimental group were loaded on the Chromium platform (10X Genomics) and libraries were constructed using a Chromium Single Cell 3' library & Gel Bead Kit V2 (10X Genomics, PN–120237) according to the manufacturer's instructions. Libraries were sequenced on an Illumina Novaseq 6000 System, using a Novaseq 6000 S2 Reagent Kit (100 cycles; 20012862, Illumina). Data analysis was performed using a Cellranger Software Suite (10X Genomics). BCL files were extracted from the sequencer and used as inputs for the cellranger pipeline to generate the digital expression matrix for each sample. Then cellranger aggr command was used to aggregate the two samples into one digital expression matrix. The matrix was analyzed using Seurat, an R package designed for single cell RNA sequencing. Specifically, cells were first filtered to have at least 300 UMIs (unique molecular identifiers), at least 100 genes and at most 50% mitochondrial gene expression; only 1 cell did not pass the filter. The filtered matrix was normalized using the Seurat function NormalizeData. Variable genes were found using the Seurat function FindVariableGenes. The matrix was scaled to regress out the sequencing depth for each cell. Variable genes that had been previously identified were used in principle component analysis (PCA) to reduce the dimensions of the data. Following this, 13 PCs were used in UMAP to further reduce the dimensions to 2. The same 13 PCs were also used to group the cells into different clusters by

the Seurat function FindClusters. Next, marker genes were found for each cluster and used to define the cell types. Subsequently, 2 clusters of TAMs (identified by co-expression of *Mrc1* and *Cd86* signature genes) were extracted and compared between the *Maoa* WT and *Maoa KO* samples. Expression distribution of immunosuppressive and immunostimulatory signature genes in *Maoa* WT and *Maoa* KO TAMs were compared and presented in violin plots.

Tumour immune dysfunction and exclusion (TIDE) computational method

TIDE analyses were conducted as previously described (*http://tide.dfci.harvard.edu)* [75]. Two functions of the TIDE computational method were used: 1) the prioritization function and 2) the survival correlation function.

The prioritization function of TIDE was used to rank a target gene by its immune dysfunction/risk score, that for TAMs was calculated as its gene expression log-fold change of M2-like/M1-like MDMs [75]. A transcriptome data set (GSE35449) was used, which was generated by microarray analysis of the gene expression profiling of *in vitro* polarized M1-like or M2-like human MDMs [76]. A score higher than 1 indicates the preferential expression of a gene in M2-like compared to M1-like human macrophages. The higher a score is, the more “prioritized” a gene is in relating to TAM immunosuppressive polarization.

The survival correlation function of TIDE was used to study the clinical data correlation between the intratumoural *MAOA* gene expression and patient survival. Four patient cohorts were analyzed: ovarian cancer (GSE26712) [78], lymphoma (GSE10846) [79], breast cancer (GSE9893) [80], and melanoma (PRJEB23709) [81]. For each patient cohort, tumour samples were divided into two groups: *MAOA*-high (samples with *MAOA* expression one standard deviation above the average) and *MAOA*-low (remaining samples) groups. The association between the intratumoural *MAOA gene expression levels and patient overall survival (OS) was computed through the two-sided Wald test in the Cox-PH regression and presented in Kaplan–Meier plots. P value indicates the comparison between the MAOA-low and MAOA-high groups, and was calculated by two-sided Wald test in a Cox-PH regression.*

Statistical analysis

*GraphPad Prism 6 (GraphPad Software) was used for the graphic representation and statistical analysis of the data. All data were presented as the mean ± standard error of the mean (SEM). A 2-tailed Student’s t test was used for comparison between groups. Multiple comparisons were performed using an ordinary 1-way ANOVA followed by Tukey’s multiple comparisons test, or using a 2-way ANOVA followed by Sidak’s multiple comparisons test. P < 0.05 was considered statistically significant. ns, not significant; *P < 0.05; **P < 0.01; ***P < 0.001. For scRNAseq data analysis, Wilcoxon-rank sum test was utilized to determine the P value between two groups.*

Benjamini-Hochberg Procedure was used to adjust the P value to reduce the false positive rate.

For the Kaplan–Meier plot of the overall patient survival for ovarian cancer, lymphoma, breast cancer, and melanoma with different MAOA levels, the P value was calculated by two-sided Wald test in a Cox-PH regression.

Reporting Summary

Further information on research design is available in the Nature Research Reporting Summary linked to this article.

Declarations

Data availability

All data associated with this study are presented in the article or Supplemental Information. The genomics data generated during this study will be available at the public repository GEO when the manuscript is published. Further information and requests for new reagents generated in this study may be directed to and will be fulfilled by the Lead Contact, Lili Yang (liliyang@ucla.edu).

Acknowledgments

We thank the University of California, Los Angeles (UCLA) animal facility for providing animal support; the UCLA AIDS Institute/CFAR Virology Core/Gene and Cell Therapy Core/Humanized Mouse Core for providing human cells and tissues and humanized mice services; the UCLA BSCRC Flow Cytometry Core Facility and D. Chen (UCLA) for cell sorting support; the UCLA Technology Center for Genomics & Bioinformatics (TCGB) facility for assisting with scRNAseq; the Laboratory of Antoni Ribas (UCLA) for providing the MC38 cell line; the Laboratory of Pin Wang (University of Southern California, Los Angeles, California, USA) for providing the B16- OVA and PG13 cell lines; and the Life Science Editors and E.L. Siegler for editing the manuscript. This work was supported by a Research Career Development Award from the STOP CANCER Foundation (to L.Y.), a BSCRC-RHF Research Award from the Rose Hills Research Foundation (to L.Y.), and an Ablon Scholars Award (to L.Y.). J.Y. is a predoctoral fellow supported by the UCLA Broad Stem Cell Research Center (BSCRC) Predoctoral Fellowship. Z.L. is a postdoctoral fellow supported by the UCLA Tumour Immunology Training Grant (USHHS Ruth L. Kirschstein Institutional National Research Service Award # T32 CA 009120). Y.L. is a predoctoral fellow supported by the UCLA Whitcome Predoctoral Fellowship in Molecular Biology.

Author information

Affiliations

Department of Microbiology, Immunology and Molecular Genetics. University of California, Los Angeles, CA 90095, United States

Yu-Chen Wang, Xi Wang, Jiaji Yu, Zhe Li, Yang Zhou, Samuel Zeng, Xiaoya Ma, Yanruide Li, Jie Huang, Angela To, Nicole Clarke & Lili Yang

Department of Molecular, Cell, and Developmental Biology, and DOE Institute for Genomics and Proteomics, University of California, Los Angeles, CA 90089, United States

Feiyang Ma & Matteo Pellegrini

Eli and Edythe Broad Center of Regeneration Medicine and Stem Cell Research. University of California, Los Angeles, CA 90095, United States

Adam Neal & Sanaz Memarzadeh

Contributions

Y-C.W. and L.Y. designed the study, analyzed the data, and wrote the manuscript. Y-C.W. performed all experiments, with the assistance from X.W. (Fig. 1, B to H, 2M, 5J, and fig. S5, B to F, S6, C and D), J.Y. (Fig. 3, L and M, and Fig. 6, K to M), F.M. and M.P. (Fig. 1, K to N and fig. S1, E to G), Z.L. (fig. S1A, and Fig. 3D, 6D, and fig. S6, E to H), Y.Z., S.Z., J.H., A.T., and N.C. (Fig. 1, B to H and Fig. 2, A to F), X.M. (Fig. 4, H to K), Y.L. (Fig. 6, K to M), A.N. and S.M. (Fig. 6N and Table S1). S.W., S.Z., and X.M. helped with critical reading of the manuscript.

L.Y. supervised the entire study.

Corresponding authors Correspondence to Lili Yang.

Ethics declarations

Competing interests

The authors declare no competing interests.

References

1. *Jenkins, R.W., Thummalapalli, R., Carter, J., Canadas, I. & Barbie, D.A. Molecular and Genomic Determinants of Response to Immune Checkpoint Inhibition in Cancer. Annu Rev Med **69**, 333-347 (2018).*

2. *Ribas, A. Releasing the Brakes on Cancer Immunotherapy. N Engl J Med **373**, 1490- 1492 (2015).*

3. *Page, D.B., Postow, M.A., Callahan, M.K., Allison, J.P. & Wolchok, J.D. Immune modulation in cancer with antibodies. Annu Rev Med **65**, 185-202 (2014).*

4. *Hodi, F.S. et al. Improved survival with ipilimumab in patients with metastatic melanoma. N Engl J Med **363**, 711-723 (2010).*

5. *Topalian, S.L. et al. Safety, activity, and immune correlates of anti-PD-1 antibody in cancer. N Engl J Med **366**, 2443-2454 (2012).*

6. *Dougan, M., Dranoff, G. & Dougan, S.K. Cancer Immunotherapy: Beyond Checkpoint Blockade. Annu Rev Canc Biol **3**, 55-75 (2019).*

7. *Sharpe, A.H. Introduction to checkpoint inhibitors and cancer immunotherapy. Immunol Rev **276**, 5-8 (2017).*

8. *Li, Y. et al. A Mini-Review for Cancer Immunotherapy: Molecular Understanding of PD-1/PD-L1 Pathway & Translational Blockade of Immune Checkpoints. Int J Mol Sci **17** (2016).*

9. *Topalian, S.L., Taube, J.M., Anders, R.A. & Pardoll, D.M. Mechanism-driven biomarkers to guide immune checkpoint blockade in cancer therapy. Nat Rev Cancer **16**, 275-287 (2016).*

10. *Baumeister, S.H., Freeman, G.J., Dranoff, G. & Sharpe, A.H. Coinhibitory Pathways in Immunotherapy for Cancer. Annu Rev Immunol **34**, 539-573 (2016).*

11. *Pardoll, D.M. The blockade of immune checkpoints in cancer immunotherapy. Nat Rev Cancer **12**, 252-264 (2012).*

12. *Ascierto, P.A., Simeone, E., Sznol, M., Fu, Y.X. & Melero, I. Clinical experiences with anti-CD137 and anti-PD1 therapeutic antibodies. Semin Oncol **37**, 508-516 (2010).*

13. *Sharpe, A.H. & Pauken, K.E. The diverse functions of the PD1 inhibitory pathway. Nat Rev Immunol **18**, 153-167 (2018).*

14. *Peranzoni, E. et al. Macrophages impede CD8 T cells from reaching tumour cells and limit the efficacy of anti-PD-1 treatment. Proc Natl Acad Sci U S A **115**, E4041-E4050 (2018).*

15. *DeNardo, D.G. et al. Leukocyte complexity predicts breast cancer survival and functionally regulates response to chemotherapy. Cancer Discov **1**, 54-67 (2011).*

16. *Cassetta, L. & Kitamura, T. Targeting Tumour-Associated Macrophages as a Potential Strategy to Enhance the Response to Immune Checkpoint Inhibitors. Front Cell Dev Biol **6**, 38 (2018).*

17. *Fujimura, T., Kambayashi, Y., Fujisawa, Y., Hidaka, T. & Aiba, S. Tumour-Associated Macrophages: Therapeutic Targets for Skin Cancer. Front Oncol **8**, 3 (2018).*

18. *Awad, R.M., De Vlaeminck, Y., Maebe, J., Goyvaerts, C. & Breckpot, K. Turn Back the TIMe: Targeting Tumour Infiltrating Myeloid Cells to Revert Cancer Progression. Front Immunol **9**, 1977 (2018).*

19. *Cannarile, M.A. et al. Colony-stimulating factor 1 receptor (CSF1R) inhibitors in cancer therapy. J Immunother Cancer **5**, 53 (2017).*

20. *Liu, Y. & Cao, X. The origin and function of tumour-associated macrophages. Cell Mol Immunol **12**, 1-4 (2015).*

21. Wynn, T.A., Chawla, A. & Pollard, J.W. Macrophage biology in development, homeostasis and disease. Nature **496**, 445-455 (2013).

22. Lavin, Y., Mortha, A., Rahman, A. & Merad, M. Regulation of macrophage development and function in peripheral tissues. Nat Rev Immunol **15**, 731-744 (2015).

23. Biswas, S.K. Metabolic Reprogramming of Immune Cells in Cancer Immunity **43**, 435-449 (2015).

24. Fujimura, T., Kakizaki, A., Furudate, S., Kambayashi, Y. & Aiba, S. Tumour-associated macrophages in skin: How to treat their heterogeneity and plasticity. J Dermatol Sci **83**, 167-173 (2016).

25. Qian, B.Z. & Pollard, J.W. Macrophage diversity enhances tumour progression and metastasis. Cell **141**, 39-51 (2010).

26. Jetten, N. et al. Anti-inflammatory M2, but not pro-inflammatory M1 macrophages promote angiogenesis in vivo. Angiogenesis **17**, 109-118 (2014).

27. DeNardo, D.G. et al. CD4(+) T cells regulate pulmonary metastasis of mammary carcinomas by enhancing protumour properties of macrophages. Cancer Cell **16**, 91-102 (2009).

28. Bordon, Y. Macrophages throw tumour cells a lifeline. Nat Rev Immunol **19**, 202-203 (2019).

29. Coussens, L.M., Zitvogel, L. & Palucka, A.K. Neutralizing tumour-promoting chronic inflammation: a magic bullet? Science **339**, 286-291 (2013).

30. Pollard, J.W. Trophic macrophages in development and disease. Nat Rev Immunol **9**, 259-270 (2009).

31. *Noy, R. & Pollard, J.W. Tumour-associated macrophages: from mechanisms to Immunity **41**, 49-61 (2014).*

32. *Arlauckas, S.P. et al. Arg1 expression defines immunosuppressive subsets of tumour- associated macrophages. Theranostics **8**, 5842-5854 (2018).*

33. *Caux, C., Ramos, R.N., Prendergast, G.C., Bendriss-Vermare, N. & Menetrier-Caux, C. A Milestone Review on How Macrophages Affect Tumour Growth. Cancer Res **76**, 6439-6442 (2016).*

34. *Gabrilovich, D.I. & Nagaraj, S. Myeloid-derived suppressor cells as regulators of the immune system. Nat Rev Immunol **9**, 162-174 (2009).*

35. *Geiger, R. et al. L-Arginine Modulates T Cell Metabolism and Enhances Survival and Anti-tumour Activity. Cell **167**, 829-842 e813 (2016).*

36. *Schuette, V. et al. Mannose receptor induces T-cell tolerance via inhibition of CD45 and up-regulation of CTLA-4. Proc Natl Acad Sci U S A **113**, 10649-10654 (2016).*

37. *Biswas, S.K. & Mantovani, A. Macrophage plasticity and interaction with lymphocyte subsets: cancer as a paradigm. Nat Immunol **11**, 889-896 (2010).*

38. *Bercovici, N., Guerin, M.V., Trautmann, A. & Donnadieu, E. The Remarkable Plasticity of Macrophages: A Chance to Fight Cancer. Front Immunol **10**, 1563 (2019).*

39. *DeNardo, D.G. & Ruffell, B. Macrophages as regulators of tumour immunity and immunotherapy. Nat Rev Immunol **19**, 369-382 (2019).*

40. *Ji, L. et al. Slc6a8-Mediated Creatine Uptake and Accumulation Reprogram Macrophage Polarization via Regulating Cytokine Responses. Immunity **51**, 272-284 e277 (2019).*

41. *Jiang, M. et al. Tumour-targeted delivery of silibinin and IPI-549 synergistically inhibit breast cancer by remodeling the microenvironment. Int J Pharm **581**, 119239 (2020).*

42. *Zhang, X., Shen, L., Liu, Q., Hou, L. & Huang, L. Inhibiting PI3 kinase-gamma in both myeloid and plasma cells remodels the suppressive tumour microenvironment in desmoplastic tumours. J Control Release **309**, 173-180 (2019).*

43. *Tiihonen, J. et al. Genetic background of extreme violent behavior. Mol Psychiatry **20**, 786-792 (2015).*

44. *Gibbons, A. American Association of Physical Anthropologists meeting. Tracking the evolutionary history of a "warrior" gene. Science **304**, 818 (2004).*

45. *Shih, J.C., Chen, K. & Ridd, M.J. Monoamine oxidase: from genes to behavior. Annu Rev Neurosci **22**, 197-217 (1999).*

46. *Brunner, H.G., Nelen, M., Breakefield, X.O., Ropers, H.H. & van Oost, B.A. Abnormal behavior associated with a point mutation in the structural gene for monoamine oxidase A. Science **262**, 578-580 (1993).*

47. *Meyer, J.H. et al. Elevated monoamine oxidase a levels in the brain: an explanation for the monoamine imbalance of major depression. Arch Gen Psychiatry **63**, 1209-1216 (2006).*

48. *Dias, V., Junn, E. & Mouradian, M.M. The role of oxidative stress in Parkinson's J Parkinsons Dis **3**, 461-491 (2013).*

49. Tong, J. et al. Brain monoamine oxidase B and A in human parkinsonian dopamine deficiency disorders. Brain **140**, 2460-2474 (2017).

50. Benson, C.A., Wong, G., Tenorio, G., Baker, G.B. & Kerr, B.J. The MAO inhibitor phenelzine can improve functional outcomes in mice with established clinical signs in experimental autoimmune encephalomyelitis (EAE). Behav Brain Res **252**, 302-311 (2013).

51. Finberg, J.P. & Rabey, J.M. Inhibitors of MAO-A and MAO-B in Psychiatry and Neurology. Front Pharmacol **7**, 340 (2016).

52. Musgrave, T. et al. The MAO inhibitor phenelzine improves functional outcomes in mice with experimental autoimmune encephalomyelitis (EAE). Brain Behav Immun **25**, 1677- 1688 (2011).

53. Bolasco, A., Carradori, S. & Fioravanti, R. Focusing on new monoamine oxidase inhibitors. Expert Opin Ther Pat **20**, 909-939 (2010).

54. Bortolato, M., Chen, K. & Shih, J.C. Monoamine oxidase inactivation: from pathophysiology to therapeutics. Adv Drug Deliv Rev **60**, 1527-1533 (2008).

55. Riederer, P. & Laux, G. MAO-inhibitors in Parkinson's Disease. Exp Neurobiol **20**, 1-17 (2011).

56. Bortolato, M. et al. Social deficits and perseverative behaviors, but not overt aggression, in MAO-A hypomorphic mice. Neuropsychopharmacology **36**, 2674-2688 (2011).

57. Zhang, Y. et al. ROS play a critical role in the differentiation of alternatively activated macrophages and the occurrence of tumour-associated macrophages. Cell Res **23**, 898- 914 (2013).

58. He, C., Ryan, A.J., Murthy, S. & Carter, A.B. Accelerated development of pulmonary fibrosis via Cu,Zn-superoxide dismutase-induced alternative activation of macrophages. J Biol Chem **288**, 20745-20757 (2013).

59. Murthy, S., Ryan, A., He, C., Mallampalli, R.K. & Carter, A.B. Rac1-mediated mitochondrial H2O2 generation regulates MMP-9 gene expression in macrophages via inhibition of SP-1 and AP-1. J Biol Chem **285**, 25062-25073 (2010).

60. Zhang, L. et al. Oxidative stress and asthma: proteome analysis of chitinase-like proteins and FIZZ1 in lung tissue and bronchoalveolar lavage fluid. J Proteome Res **8**, 1631-1638 (2009).

61. Vats, D. et al. Oxidative metabolism and PGC-1beta attenuate macrophage-mediated inflammation. Cell Metab **4**, 13-24 (2006).

62. Fu, C. et al. Activation of the IL-4/STAT6 Signaling Pathway Promotes Lung Cancer Progression by Increasing M2 Myeloid Cells. Front Immunol **10**, 2638 (2019).

63. Van Dyken, S.J. & Locksley, R.M. Interleukin-4- and interleukin-13-mediated alternatively activated macrophages: roles in homeostasis and disease. Annu Rev Immunol **31**, 317-343 (2013).

64. Bhattacharjee, A. et al. IL-4 and IL-13 employ discrete signaling pathways for target gene expression in alternatively activated monocytes/macrophages. Free Radic Biol Med **54**, 1-16 (2013).

65. Nelms, K., Keegan, A.D., Zamorano, J., Ryan, J.J. & Paul, W.E. The IL-4 receptor: signaling mechanisms and biologic functions. Annu Rev Immunol **17**, 701-738 (1999).

66. Dwivedi, G., Gran, M.A., Bagchi, P. & Kemp, M.L. Dynamic Redox Regulation of IL-4 Signaling. PLoS Comput Biol **11**, e1004582 (2015).

67. Park, S.J. et al. Astrocytes, but not microglia, rapidly sense H(2)O(2)via STAT6 phosphorylation, resulting in cyclooxygenase-2 expression and prostaglandin release. J Immunol **188**, 5132-5141 (2012).

68. Duhe, R.J. Redox regulation of Janus kinase: The elephant in the room. JAKSTAT **2**, e26141 (2013).

69. Duan, W. et al. New role of JAK2/STAT3 signaling in endothelial cell oxidative stress injury and protective effect of melatonin. PLoS One **8**, e57941 (2013).

70. Abe, J. & Berk, B.C. Fyn and JAK2 mediate Ras activation by reactive oxygen species. J Biol Chem **274**, 21003-21010 (1999).

71. Simon, A.R., Rai, U., Fanburg, B.L. & Cochran, B.H. Activation of the JAK-STAT pathway by reactive oxygen species. Am J Physiol **275**, C1640-1652 (1998).

72. Wimbiscus, M., Kostenko, O. & Malone, D. MAO inhibitors: risks, benefits, and Cleve Clin J Med **77**, 859-882 (2010).

73. Bruhwyler, J., Liegeois, J.F. & Geczy, J. Pirlindole: a selective reversible inhibitor of monoamine oxidase A. A review of its preclinical properties. Pharmacol Res **36**, 23-33 (1997).

74. Homet Moreno, B. et al. Response to Programmed Cell Death-1 Blockade in a Murine Melanoma Syngeneic Model Requires Costimulation, CD4, and CD8 T Cells. Cancer Immunol Res **4**, 845-857 (2016).

75. Jiang, P. et al. Signatures of T cell dysfunction and exclusion predict cancer immunotherapy response. Nat Med **24**, 1550-1558 (2018).

76. Beyer, M. et al. High-resolution transcriptome of human macrophages. PLoS One **7**, e45466 (2012).

77. Thomas, R. et al. NY-ESO-1 Based Immunotherapy of Cancer: Current Front Immunol **9**, 947 (2018).

78. Bonome, T. et al. A gene signature predicting for survival in suboptimally debulked patients with ovarian cancer. Cancer Res **68**, 5478-5486 (2008).

79. Lenz, G. et al. Stromal gene signatures in large-B-cell lymphomas. N Engl J Med **359**, 2313-2323 (2008).

80. Chanrion, M. et al. A gene expression signature that can predict the recurrence of tamoxifen-treated primary breast cancer. Clin Cancer Res **14**, 1744-1752 (2008).

81. Gide, T.N. et al. Distinct Immune Cell Populations Define Response to Anti-PD-1 Monotherapy and Anti-PD-1/Anti-CTLA-4 Combined Therapy. Cancer Cell **35**, 238-255 e236 (2019).

82. Talbot, S., Foster, S.L. & Woolf, C.J. Neuroimmunity: Physiology and Pathology. Annu Rev Immunol **34**, 421-447 (2016).

83. Franco, R., Pacheco, R., Lluis, C., Ahern, G.P. & O'Connell, P.J. The emergence of neurotransmitters as immune modulators. Trends Immunol **28**, 400-407 (2007).

84. Kerage, D., Sloan, E.K., Mattarollo, S.R. & McCombe, P.A. Interaction of neurotransmitters and neurochemicals with lymphocytes. J Neuroimmunol **332**, 99-111 (2019).

85. Yang, L. & Zhang, Y. Tumour-associated macrophages: from basic research to clinical application. J Hematol Oncol **10**, 58 (2017).

86. Guerriero, J.L. et al. Class IIa HDAC inhibition reduces breast tumours and metastases through anti-tumour macrophages. Nature **543**, 428-432 (2017).

87. Beatty, G.L. et al. CD40 agonists alter tumour stroma and show efficacy against pancreatic carcinoma in mice and humans. Science **331**, 1612-1616 (2011).

88. Kaneda, M.M. et al. PI3Kgamma is a molecular switch that controls immune suppression. Nature **539**, 437-442 (2016).

89. Zhang, J.Q. et al. Macrophages and CD8(+) T Cells Mediate the Antitumour Efficacy of Combined CD40 Ligation and Imatinib Therapy in Gastrointestinal Stromal Tumours. Cancer Immunol Res **6**, 434-447 (2018).

90. Falkenberg, K.J. & Johnstone, R.W. Histone deacetylases and their inhibitors in cancer, neurological diseases and immune disorders. Nat Rev Drug Discov **13**, 673-691 (2014).

91. Ghizzoni, M., Haisma, H.J., Maarsingh, H. & Dekker, F.J. Histone acetyltransferases are crucial regulators in NF-kappaB mediated inflammation. Drug Discov Today **16**, 504-511 (2011).

92. Sai, J. et al. PI3K Inhibition Reduces Mammary Tumour Growth and Facilitates Antitumour Immunity and Anti-PD1 Responses. Clin Cancer Res **23**, 3371-3384 (2017).

93. Zheng, W. & Pollard, J.W. Inhibiting macrophage PI3Kgamma to enhance immunotherapy. Cell Res **26**, 1267-1268 (2016).

94. Schein, C.H. Repurposing approved drugs on the pathway to novel therapies. Med Res Rev (2019).

95. Jessen, L., Kovalick, L.J. & Azzaro, A.J. The selegiline transdermal system (emsam): a therapeutic option for the treatment of major depressive disorder. P T **33**, 212-246 (2008).

96. Shoval, G. et al. Adherence to antidepressant medications is associated with reduced premature mortality in patients with cancer: A nationwide cohort study. Depress Anxiety **36**, 921-929 (2019).

97. Liu, Y. et al. In situ modulation of dendritic cells by injectable thermosensitive hydrogels for cancer vaccines in mice. Biomacromolecules **15**, 3836-3845 (2014).

98. Bethune, M.T. et al. Isolation and characterization of NY-ESO-1-specific T cell receptors restricted on various MHC molecules. Proc Natl Acad Sci U S A **115**, E10702-E10711 (2018).

99. Di Biase, S. et al. Creatine uptake regulates CD8 T cell antitumour immunity. J Exp Med **216**, 2869-2882 (2019).

100. Smith, D.J. et al. Genetic engineering of hematopoietic stem cells to generate invariant natural killer T cells. Proc Natl Acad Sci U S A **112**, 1523-1528 (2015).

101. Li, B. et al. miR-146a modulates autoreactive Th17 cell differentiation and regulates organ-specific autoimmunity. J Clin Invest **127**, 3702-3716 (2017).

102. Smith, D.J. et al. Propagating Humanized BLT Mice for the Study of Human Immunology and Immunotherapy. Stem Cells Dev **25**, 1863-1873 (2016).

Figures

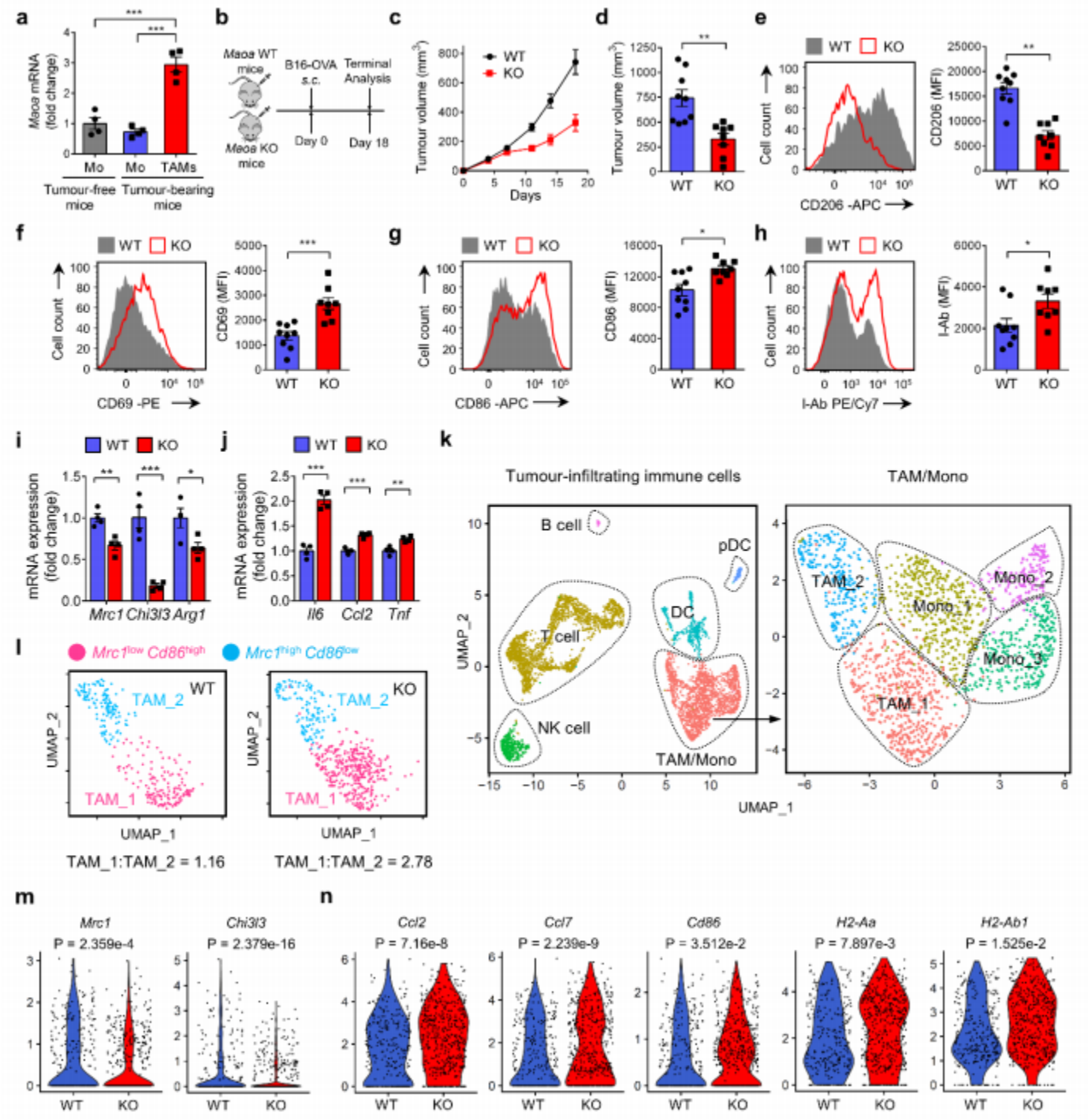

Figure 1

MAO-A-deficient mice show reduced tumour growth associated with altered TAM polarization. a, QPCR analyses of Maoa mRNA expression in TAMs isolated from wildtype mice bearing B16-OVA tumours. Monocytes (Mo) isolated from tumour-free and tumour-bearing mice were included as controls. N = 4. b-d, Growth of B16-OVA tumours in Maoa WT and Maoa KO mice. (b) Experimental design. (c) Tumour growth. (d) Tumour volume at day 18. N = 8-9. e-j, Phenotype of TAMs isolated from Maoa WT and Maoa KO mice bearing B16-OVA tumours, at day 18 post tumour challenge. (e-h) FACS analyses of CD206 (e), CD69 (f), CD86 (g), and I-Ab (h) expression on TAMs (n = 8-9). MFI, mean fluorescence intensity. (i, j)

*QPCR analyses of immunosuppressive (Mrc1, Chi3l3, and Arg1; i) and immunostimulatory (Il6, Ccl2, and Tnf; j) signature gene mRNA expression in TAMs (n = 4). k-n, scRNAseq analyses of tumour-infiltrating immune cells (TIIs) isolated from Maoa WT and Maoa KO mice bearing B16-OVA tumours, at day 14 post tumour challenge. (k) Uniform Manifold Approximation and Projection (UMAP) of single TIIs showing the formation of 6 cell clusters TAM2, Mono1, Mono2, and Mono3) from the TAM/Mono subpopulation. Each dot represents one single cell and is colored according to cell types. Mono, monocyte; NK, natural killer cell; DC, dendritic cell; pDC, plasmacytoid dendritic cell. (l) UMAP of the TAM subpopulation, showing the formation of two is colored according to cell clusters. Ratios of TAM1:TAM2 are presented. (m, n) Violin plots showing the expression distribution of immunosuppressive (Mrc1 and Chi3l3; m) and immunostimulatory (Ccl2, Ccl7, Cd86, H2-Aa, and H2-Ab1; n) signature genes in single TAMs. Each dot represents an individual cell. Representative of 1 (k-n), 3 (a), and 5 (b-j) experiments. All data are presented as the mean ± SEM. *P < 0.05, **P < 0.01, and ***P < 0.001, by 1-way ANOVA (a) or by Student's t test (c-j). P values of violin plots were determined by Wilcoxon rank sum test (m, n).*

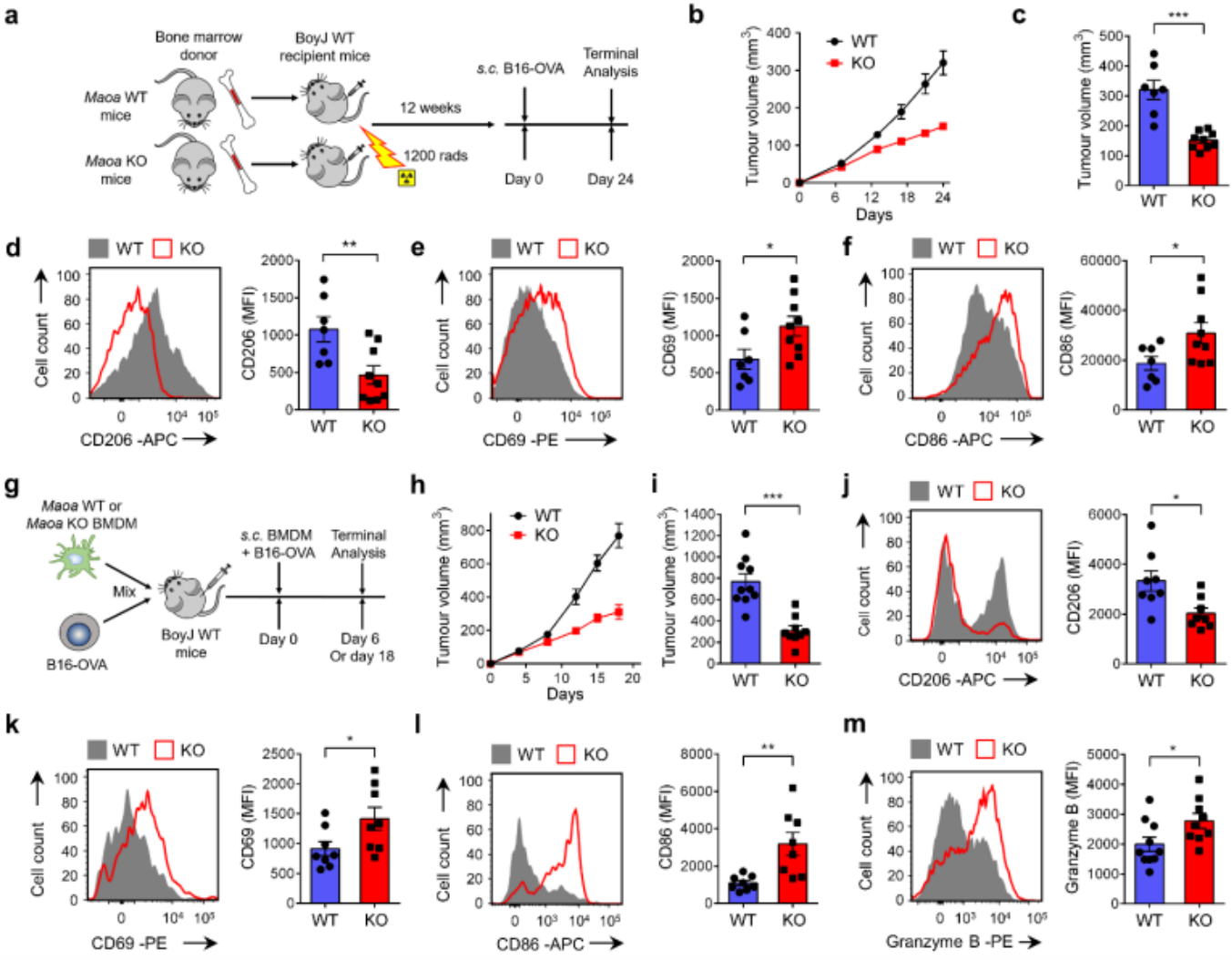

Figure 2

*MAO-A directly regulates TAM polarization and influences TAM-associated antitumour T cell reactivity. a-f, Studying B16-OVA tumour growth and TAM phenotype in BoyJ (CD45.1) wildtype mice reconstituted with bone marrow cells isolated from either Maoa WT or Maoa KO donor mice (denoted as WT or KO experimental mice, respectively). (a) Experimental design. (b) Tumour growth. (c) Tumour volume at day 24. (d-f) FACS analyses of CD206 (d), CD69 (e), and CD86 (f) expression on TAMs at day 24. N = 8-9. g-m, Studying B16-OVA tumour growth and antitumour T cell reactivity in a Tumour-TAM Co- Inoculation in vivo experiment. BoyJ wildtype mice received s.c. inoculation of B16-OVA tumour cells mixed with either Maoa WT or Maoa KO BMDMs (denoted as WT or KO experimental mice, respectively). BMDM, bone marrow-derived macrophage. (g) Experimental design. (h) Tumour growth (n = 9-10). (i) Tumour volume at day 18 (n = 9-10). (j-l) FACS analyses of CD206 (j), CD69 (k), and CD86 (l) (m) FACS analyses of intracellular Granzyme B production in tumour-infiltrating CD45.1+CD8+ T cells at day 18 (n = 9-10). Representative of 3 experiments. All data are presented as the mean ± SEM. *P < 0.05, **P < 0.01, and ***P < 0.001, by Student's t test.*

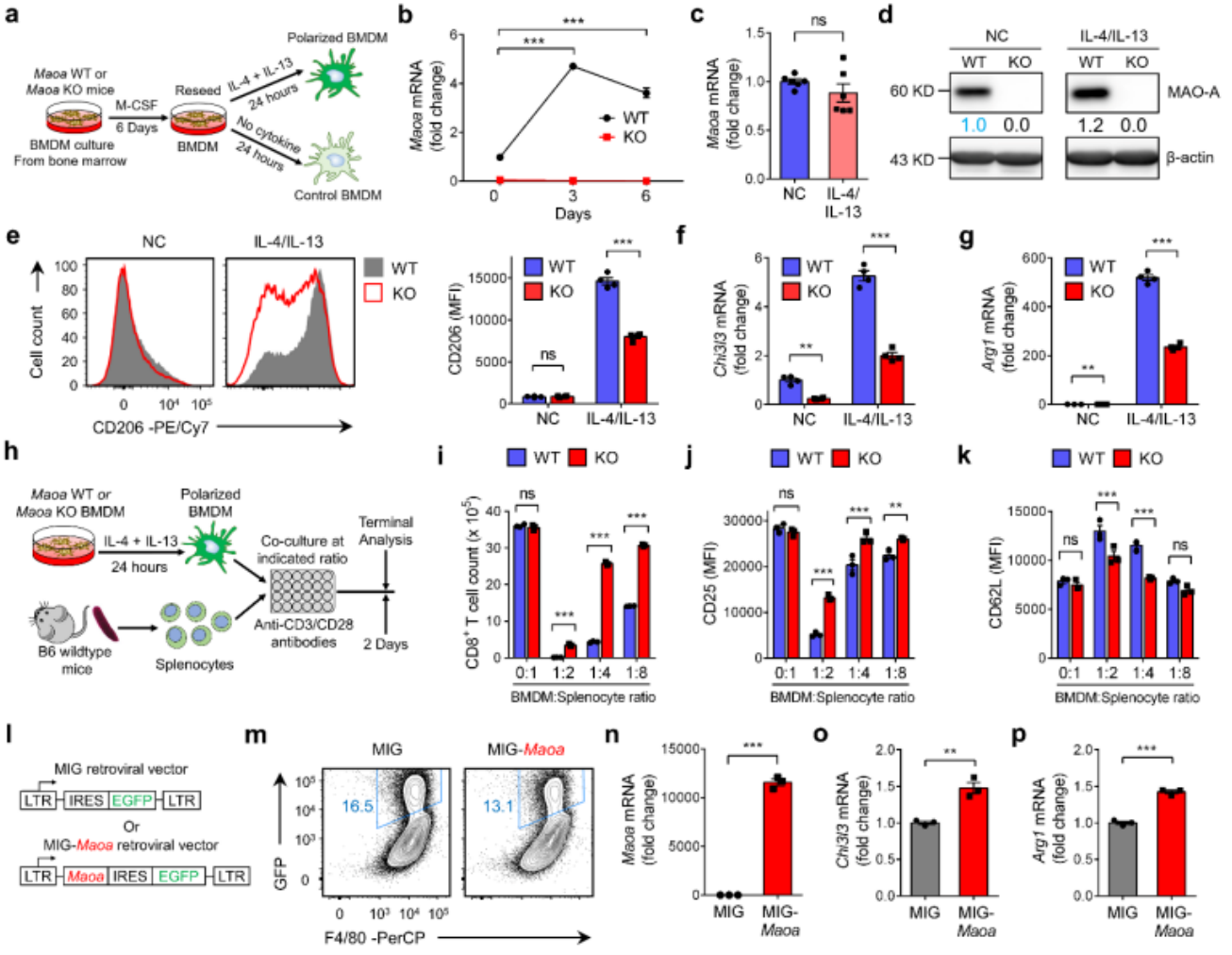

Figure 3

*MAO-A promotes macrophage immunosuppressive polarization. a-g, Studying the in vitro differentiation and IL-4/IL-13-induced polarization of Maoa WT (WT) and Maoa KO (KO) BMDMs. (a) Experimental design. (b,c) QPCR analyses of Maoa mRNA expression over the 6-day BMDM differentiation culture (b) and IL-4/IL-13-induced polarization (c) (n = 6). (d). Western blot analyses of MAOA protein expression in the indicated BMDMs. (e) FACS analyses of CD206 expression on the indicated BMDMs (n = 4). (f,g) QPCR analyses of Chi3l3 (f) and Arg1 (g) mRNA expression in the indicated BMDMs (n = 4). NC, no cytokine control BMDMs; IL-4/IL-13, IL-4 and IL-13-polarized BMDMs. h-k, Studying the T cell suppression function of Maoa WT (WT) and Maoa KO (KO) IL-4/IL-13- \polarized BMDMs in an in vitro macrophage/T cell co-culture assay (n = 3). (h) Experimental design. (i) FACS quantification of CD8+ T cells (identified as TCR+CD4-CD8+ cells). (j,k) FACS analyses of CD25 (j) and CD62L (k) expression on CD8+ T cells. l-p, Studying the IL-4/IL-13-induced polarization of Maoa KO BMDMs with MAO-A overexpression (n = 3). In vitro-cultured Maoa KO BMDMs were transduced with either a MIG-Maoa retrovector or a MIG mock retrovector, polarized with IL-4/IL-13, followed by FACS sorting of GFP+ Maoa KO BMDMs for further analyses. (l) Schematics of the MIG and MIG-Maoa retrovectors. (m) FACS analyses of prior-to-sorting Maoa KO BMDMS, showing retrovector transduction efficiency (measured as %GFP+ cells). (n-p) QPCR analyses of sorted GFP+ Maoa KO BMDMs, showing the mRNA expression of Maoa (n), Chi3l3 (o), and Arg1 (p). Representative of 3 (h-k, l-p) and 4 (a-g) experiments. All data are presented as the mean ± SEM. ns, not significant, **P < 0.01, and ***P < 0.001, by 1-way ANOVA (b), 2-way ANOVA (e-g, i-k), or Student's t test (c, n-p).*

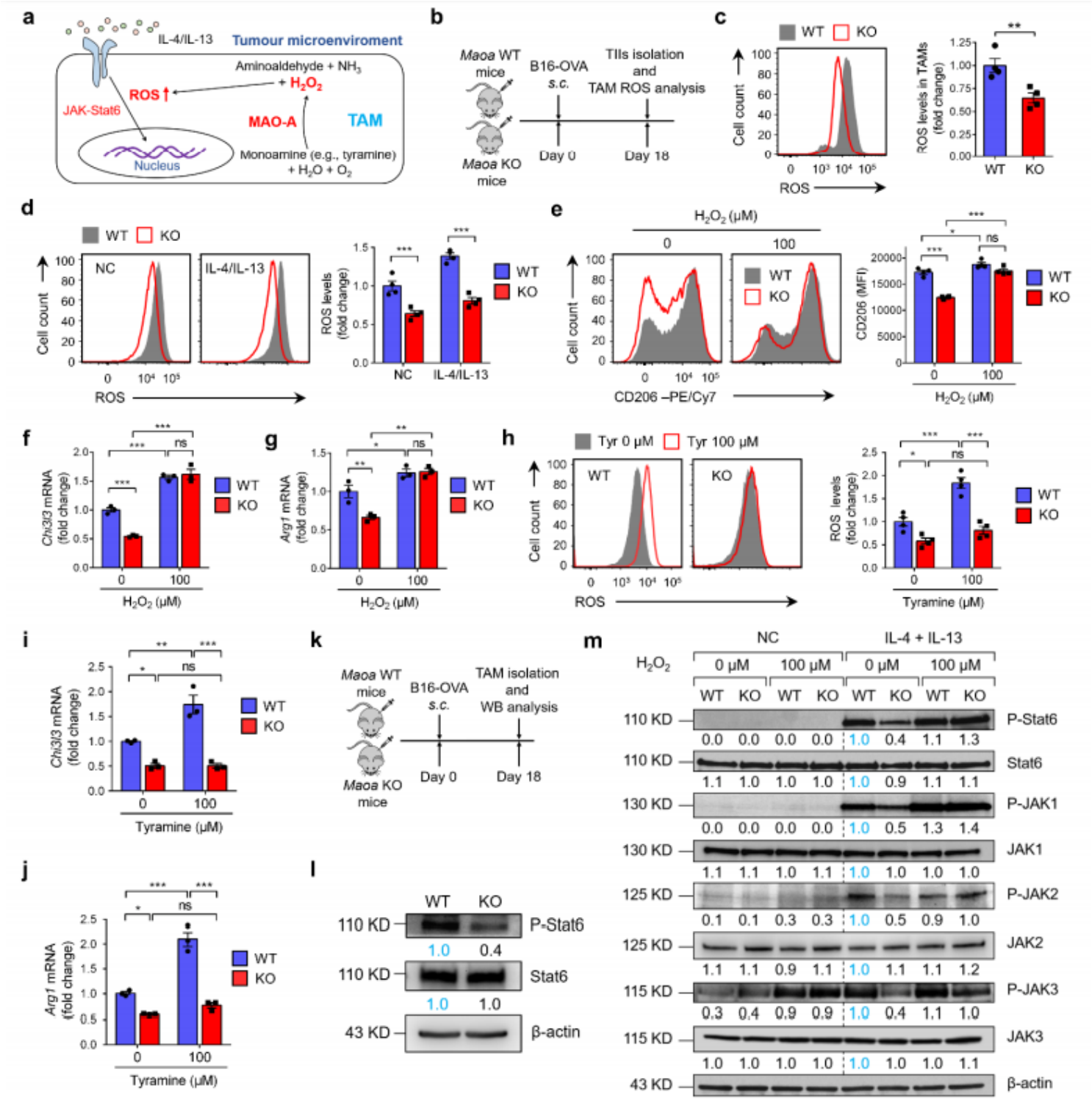

Figure 4

MAO-A promotes macrophage immunosuppressive polarization via ROS upregulation. a, Schematics showing the enzymatic activity of MAO-A in a TAM. MAO-A breaks down monoamines and generates hydrogen peroxide (H2O2) as a byproduct, thereby increasing reactive oxygen species (ROS) levels in a TAM. b,c, Studying the in vivo ROS levels in TAMs isolated from Mao WT and Mao KO mice bearing B16-OVA tumours (n = 4). (b) Experimental design. (c) FACS analyses of ROS levels in Maoa WT and Maoa KO TAMs at day 18. TAMs were gated as the CD45.2+CD11b+Ly6G-Ly6C-/lowF4/80+ cells of total tumour-

*infiltrating immune cells (TIIs). d, FACS analyses of ROS levels in in vitro-cultured Maoa WT and Maoa KO BMDMs, without or without IL-4/IL-13 polarization for 24 hours (n = 4). NC, no cytokine-treated control BMDMs; IL-4/IL- 13, IL-4/IL-13-polarized BMDMs. e-g, Studying the phenotype of IL-4/IL-13-polarized Maoa WT and Maoa KO BMDMs with or without H2O2 treatment (n = 3). BMDMs were treated with H2O2 for 30 minutes prior to IL-4/IL-13 polarization for 24 hours. (e) FACS analyses of CD206 expression on BMDMs. (f,g) QPCR analyses of Chi3l3 (f) and Arg1 (g) mRNA expression in BMDMs. h-j, Studying the phenotype of IL-4/IL-13-polarized Maoa WT and Maoa KO BMDMs with or without tyramine supplement (n = 3). BMDMs were treated with tyramine for 30 minutes prior to IL-4/IL-13 polarization for 24 hours. (h) FACS analyses of ROS levels in BMDMs. (i,j) QPCR analyses of Chi3l3 (i) and Arg1 (j) mRNA expression in BMDMs. k,l, Studying the in vivo Stat6 signaling in TAMs isolated from Mao WT and Mao KO mice bearing B16-OVA tumours (combined from 5 mice per group). (k) Experimental design. (l) Western blot analyses of Stat6 phosphorylation in TAMs at day 18. TAMs were FACS sorted as the DAPI-CD45.2+CD11b+Ly6G-Ly6C-/lowF4/80+ cells from total TIIs. m, Western blot analyses of JAK-Stat6 signaling in in vitro-cultured Maoa WT and Maoa KO BMDMs, with or without IL-4/IL-13 polarization and H2O2 treatment. BMDMs were treated with H2O2 for 30 minutes prior to IL-4/IL-13 stimulation for another 30 minutes. Representative of 3 experiments. All data are presented as the mean ± SEM. ns, not significant, *P < 0.05, **P < 0.01, and ***P < 0.001, by 2-way ANOVA (d-j) or by Student's t test (c).*

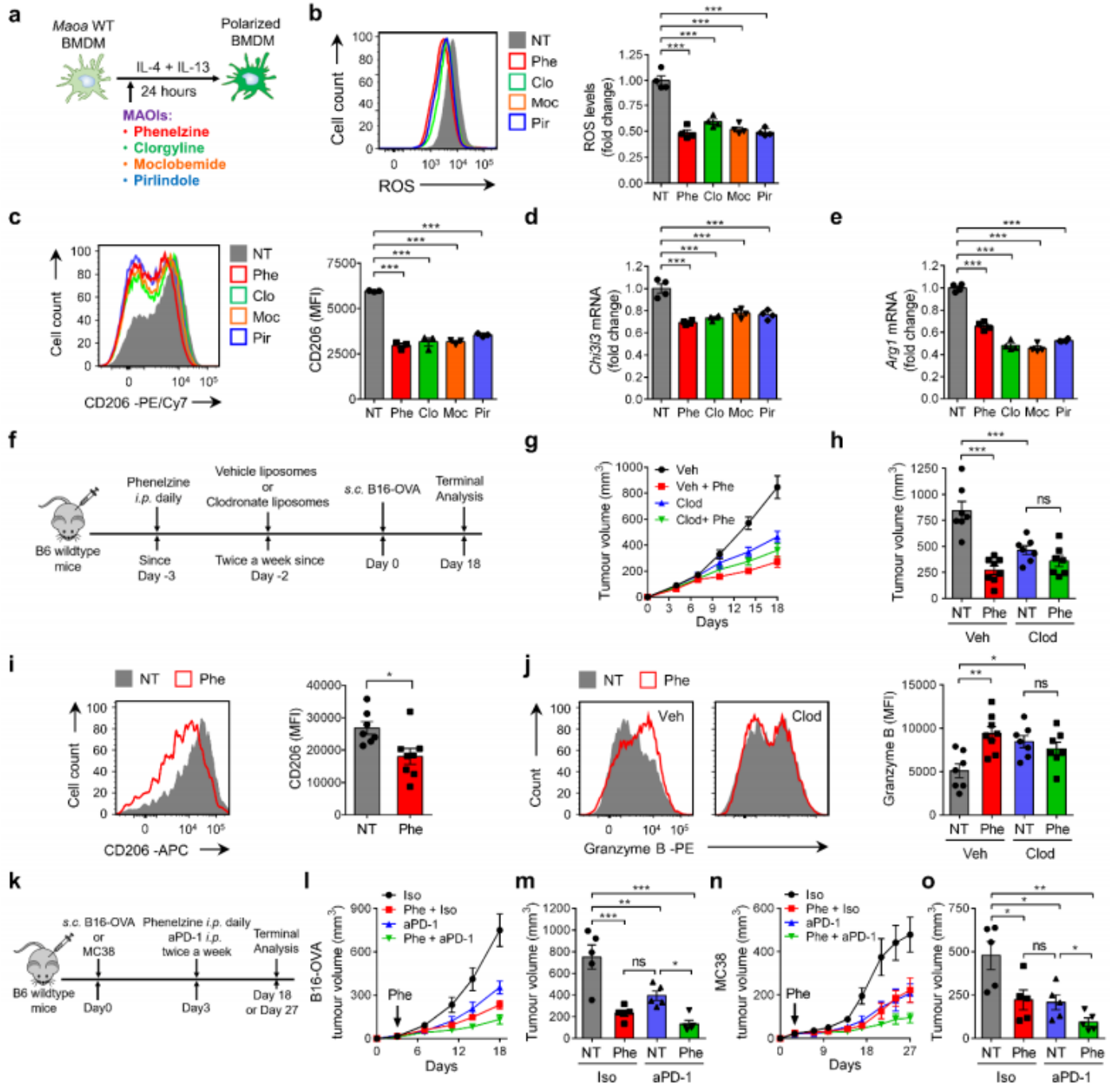

Figure 5

MAO-A blockade for cancer immunotherapy- syngeneic mouse tumour model studies. a-e, Studying the effect of MAOI treatment on IL-4/IL-13-induced BMDM polarization in vitro (n = 4). (a) Experimental design. Wildtype BMDMs were stimulated with IL-4/IL-13 with or without MAOI treatment. MAOIs (monoamine oxidase inhibitors) studied were phenelzine (Phe; 20 μM), clorgyline (Clo; 20 μM), moclobemide (Moc; 200 μM), and pirlindole (Pir; 20 μM). NT, no MAOI treatment. (b) FACS analyses of ROS levels in BMDMs. (c) FACS analyses of CD206 expression on BMDMs. (d,e) QPCR analyses of Chi3l3 (d) and Arg1 (e) mRNA expression in BMDMs. f-j, Studying the TAM-related cancer immunotherapy

*potential of MAOI treatment in a B16-OVA melanoma syngeneic mouse tumour model (n = 7-8). (f) Experimental design. B6 wildtype mice were treated with clodronate liposomes (Clod) to serve as TAM-depleted experimental mice, or treated with vehicle liposomes (Veh) to serve as TAM-intact control mice. Phe, phenelzine treatment; NT, no phenelzine treatment. (g) Tumour growth. (h) Tumour volume at day 18. (i) FACS analyses of CD206 expression on TAMs of TAM-intact experimental mice. (j) FACS analyses of intracellular Granzyme B production in tumour-infiltrating CD8+ T cells of all experimental mice. k-o, Studying the cancer therapy potential of MAOI treatment in combination with anti-PD-1 treatment in the B16-OVA melanoma and MC38 colon cancer syngeneic mouse tumour models (n = 5). (k) Experimental design. Tumour-bearing mice were treated with anti-PD-1 antibody (aPD-1) or isotype control (Iso), together with or without phenelzine (Phe) treatment. NT, no Phe treatment. (l) B16-OVA tumour growth. (m) B16-OVA tumour volume at day 18. (n) MC38 tumour growth. (o) MC38 tumour volume at day 27. Representative of 3 experiments. All data are presented as the mean ± SEM. ns, not significant, *P < 0.05, **P < 0.01, and ***P < 0.001, by 1-way ANOVA (b-e, h, j, m, o) or by Student's t test (i).*

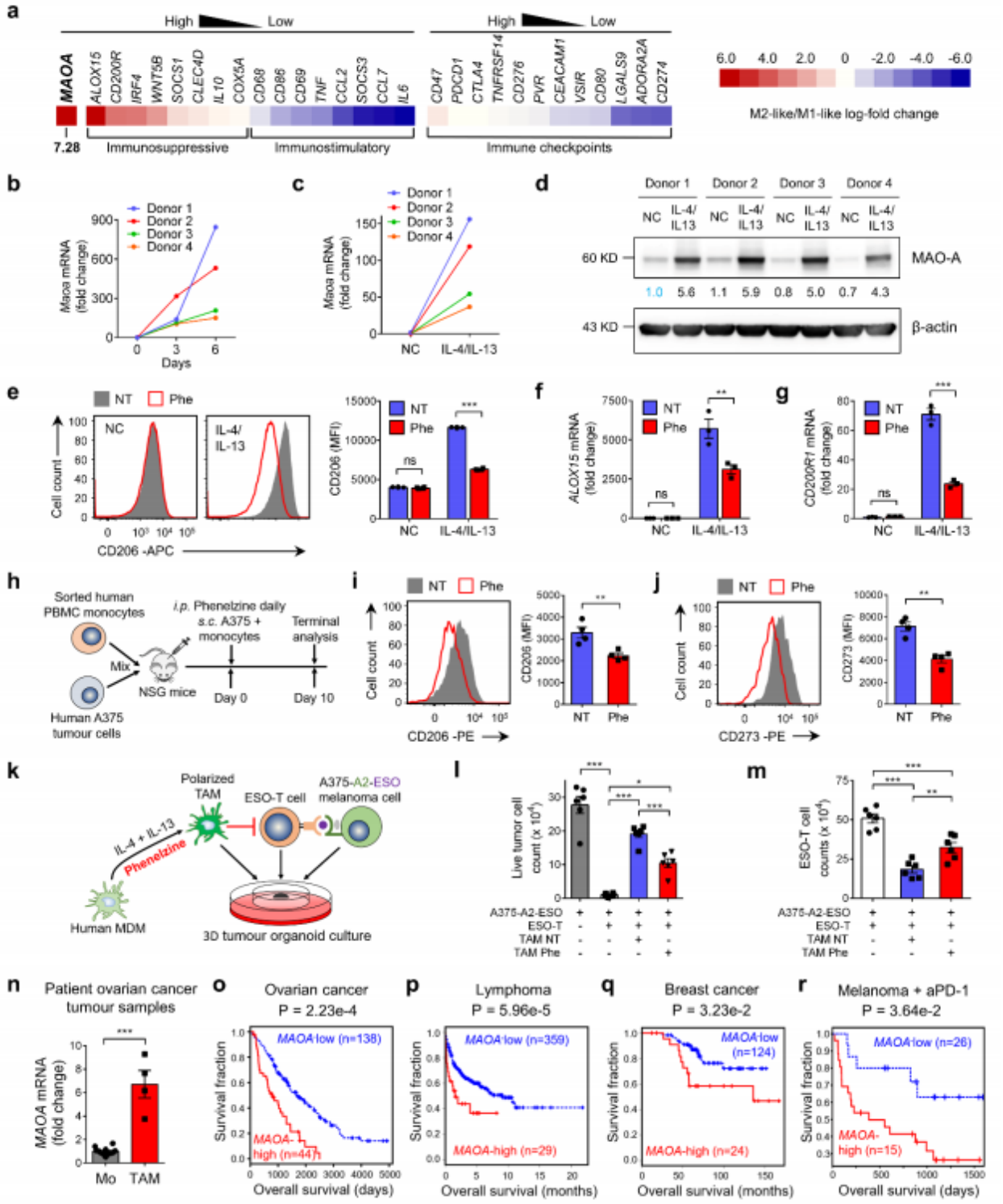

Figure 6

MAO-A blockade for cancer immunotherapy- human TAM and clinical data correlation studies. a, Studying the MAOA gene expression in human M1- and M2-like macrophages. A transcriptome data set (GSE35449) was analyzed using the prioritization function of a Tumour Immune Dysfunction and Exclusion (TIDE) computational method. Heatmaps are presented, showing the M2-like/M1-like mRNA fold change of MAOA gene as well as a selected group of immunosuppressive, immunostimulatory, and

*immune checkpoints signature genes. b-d, Studying the MAO-A expression in in vitro differentiated and IL-4/IL-13-polarized human monocyte-derived macrophages (MDMs; n = 4). MDMs were generated by culturing healthy donor peripheral blood monocytes over 6 days, followed by stimulation with IL-4 and IL-13 for another 2 days. NC, no cytokine stimulation. (b,c) QPCR analyses of MAOA mRNA expression in MDMs over the 6-day MDM differentiation culture (b) and post the IL-4/IL-13-induced polarization (c). (d) Western blot analyses of MAO-A protein expression in IL-4/IL-13-polarized MDMs. e-g, Studying the in vitro polarization of human MDMs (n = 3). MDMs were stimulated with IL-4/IL-13 for 2 days, in the presence or absence of phenelzine (Phe, 20μM) treatment. NC, no cytokine stimulation; NT, no phenelzine treatment. (e) FACS analyses of CD206 expression on MDMs. (f,g) QPCR analyses ALOX15 (f) and CD200R1 (g) mRNA expression in MDMs. h-j, Studying the in vivo polarization of human macrophages in a human Tumour-TAM Co-Inoculation xenograft mouse model (n = 4). (h) Experimental design. FACS-sorted healthy donor peripheral blood monocytes were mixed with human A375 melanoma cells and s.c. injected into NSG mice to form solid tumours, with or without phenelzine treatment (Phe or NT). (i,j) FACS analyses of CD206 (i) and CD273 j) expression on TAMs (gated as hCD45+hCD11b+hCD14+ cells of total TIIs) isolated from experimental mice at day 10. k-m, Studying the in vitro efficacy of phenelzine in reprogramming human TAMs and enhancing human T cell antitumour reactivity (n = 6). (k) Schematics showing an in vitro 3D human tumour/TAM/T cell organoid culture. A375-A2-ESO, human A375 melanoma cell line engineered to express an NY-ESO-1 tumour antigen as well as its matching HLA-A2 molecule; ESO-T, human peripheral blood CD8 T cells engineered to express an NY-ESO-1-specific TCR; Polarized TAM, human MDMs polarized in vitro with IL-4/IL-13 in the presence or absence of phenelzine treatment (denoted as TAM Phe or TAM NT, respectively). Cells were mixed and cultured as organoids for two days before analysis. (l,m) FACS quantification of live tumour cells (gated as hCD45- cells) and ESO-T cells (gated as hCD45+hCD8+ESO-TCR+ cells). n, QPCR analyses of MAOA mRNA expression in human TAMs isolated from ovarian cancer patient tumour samples (n = 4). Monocytes isolated from random healthy donor peripheral blood were included as controls (n = 10). Mo, monocyte. o-r, Clinical data correlation studies. The correlation function of a TIDE computational method was utilized. The association between the intratumoural MAOA gene expression levels and overall survival (OS) of cancer patients was computed through the two-sided Wald test in the Cox-PH regression. For each patient cohort, tumour samples were divided into the MAOA-high (samples with MAOA expression one standard deviation above the average) and MAOA-low (remaining samples) groups, followed by analysing the OS of each group. TIDE analyses of an ovarian cancer patient cohort (GSE26712, n = 182; o), a lymphoma patient cohort (GSE10846, n = 388; p), a breast cancers patient cohort (GSE9893, n = 148; q), and a melanoma patient cohort with anti-PD-1 therapy (PRJEB23709, n = 41; r). Representative of 1 (n), 2 (b-d, h-j) and 3 (e-g, k-m) experiments. All data are presented as the mean ± SEM. ns, not significant, *P < 0.05, **P < 0.01, and ***P < 0.001, by 1-way ANOVA (l, m), 2-way ANOVA (e-g), or by Student's t test (i, j, n). For Kaplan-Meier plots, the P value was calculated by two-sided Wald test in a Cox-PH regression (o-r).*

Supplementary Files

This is a list of supplementary files associated with this preprint. Click to download.

- *SupplementaryInformationTargetingmonoamineoxidase.pdf*